Eustatic knickpoint dynamics in an uplifting sequence of coral reef terraces, Sumba Island, Indonesia

Denovan Chauveau, Christine Authemayou, Stéphane Molliex, Vincent Godard, Lucilla Benedetti, Kevin Pedoja, Laurent Husson, Sri Yudawati Cahyarini

▶ To cite this version:

Denovan Chauveau, Christine Authemayou, Stéphane Molliex, Vincent Godard, Lucilla Benedetti, et al.. Eustatic knickpoint dynamics in an uplifting sequence of coral reef terraces, Sumba Island, Indonesia. Geomorphology, 2021, 393, pp.107936. ⟨10.1016/j.geomorph.2021.107936⟩. ⟨hal-03350591⟩

HAL Id: hal-03350591

https://normandie-univ.hal.science/hal-03350591v1

Submitted on 16 Oct 2023

Eustatic knickpoint dynamics in an uplifting sequence of coral reef terraces, Sumba Island, Indonesia

Denovan Chauveau[a], Christine Authemayou[a], Stéphane Molliex[a], Vincent Godard[b], Lucilla Benedetti[b], Kevin Pedoja[c], Laurent Husson[d], Sri Yudawati Cahyarini[e], A.S.T.E.R. Team[b]

[a]LGO, IUEM, CNRS, UMR 6538, Université de Bretagne Occidentale, UBO, Plouzané, France
[b]CEREGE, CNRS-IRD, UMR 34, Aix-Marseille Université, Aix-en-Provence, France
[c]M2C, CNRS, UMR 6143, Université de Caen, Caen, France
[d]ISTerre, CNRS, UMR 5275, Université de Grenoble Alpes, Grenoble, France
[e]Research Center for Geotechnology, Indonesian Institute of sciences, LIPI, Bandung, Indonésie

Keywords

Eustatic knickpoint; coral reef terrace; alluvial erosion; ^{36}Cl cosmogenic denudation rates.

Abbreviations

Coral Reef Terrace (CRT); Marine Isotopic Stage (MIS); Cosmogenic Nuclide ^{36}Cl Concentration (CNC); Digital Elevation Model (DEM).

Abstract

An emerged coral reef terrace sequence flanks the northern coast of Sumba Island in Indonesia. The sequence was created by the joint effects of uplift and Quaternary sea level oscillations. Since its emergence, it undergoes chemical erosion, which is facilitated by its carbonate lithology. The morphology is dissected by multiple catchments drained by deep canyons, whose stream profiles display several knickpoints. We applied a multi-methods approach using high-resolution topographic data (Pleiades imagery), geomorphological analysis and denudation rates derived from ^{36}Cl cosmogenic nuclide concentrations to characterize the dynamics of these coastal drainages. We specifically investigate (1) the channel response to eustatic forcing, by analyzing knickpoint dynamics along a longitudinal river profile, and (2) the control of internal and external forcing over the catchment-scale erosion. Firstly, knickpoints form at the distal edge of the emergent reef at each regressive stage following a sea level highstand. The knickpoint propagates and rotates upward by regressive erosion. Knickpoint propagation rate decreases sharply over time until it becomes negligible before the next sea-level rise, which implies a marked decline in knickpoint retreat rate before its resorption. We attribute the inability of the river at Cape Laundi to fully propagate eustatic oscillations to its low stream discharge and low sediment supply, related to its small drainage area, to the karstic nature of the coral reef terraces composing the sequence, and to the high frequency of eustatic forcing. Secondly, average denudation rates calculated from ^{36}Cl cosmogenic nuclide concentrations of sands collected at the outlet of five catchments draining the sequence amount to 69 ± 16 mm.ka^{-1}. We emphasize the role of canyon areas in driving the denudation of the major catchments. However, no first-order correlation has been observed between catchment metrics, uplift rates and denudation rates. Finally, our correlations between catchment finite eroded volumes and uplift rates highlight the

tendency of catchments to widen with low uplift rate and to lengthen while incising the sequence deeply with higher uplift rates.

1. Introduction

Rivers are relentlessly adapting to tectonic, climatic, eustatic, lithologic, and biologic conditions by modulating their erosion or sedimentation dynamics. A river responds to an extrinsic base-level drop by an upstream propagation of an incision wave (e.g., Whipple and Tucker, 1999; Montgomery and Brandon, 2002; Wobus et al., 2006; Kirby and Whipple; 2012). As the incision propagates upstream, it isolates the downstream region that is adjusted or adjusting to the new forcing conditions and the upstream relict region that retains topographic features adjusted to the initial or background forcing (Whipple and Tucker, 1999; Schoenbohm et al., 2004; Crosby and Whipple, 2006; Reinhardt et al., 2007; Berlin and Anderson, 2007; Whittaker, 2012). The river will be in a transient situation until the upstream relict region disappears. The discrete and mobile boundary between the two regions is marked by upstream-migrating steep reaches, called knickpoints, or more properly knickzones - the knickpoint being the upper break in slope from shallow to steep. Knickpoints can generate large variations in denudation rates within the catchment (e.g., Willenbring et al., 2013). Investigating the geometry of transient channels, coupled with quantified stream incision rates allows for diagnosis of active fluvial processes and to better characterize erosion laws and their controlling parameters (e.g., upstream drainage area; local channel gradient; dimensional erosion efficiency factor; e.g., Whipple and Tucker, 2002; Godard et al., 2019). In that respect, coastal areas are especially interesting because they are exposed to eustatic base-level changes (Gardner, 1983;

Snyder et al., 2002; Loget and Van Den Driessche, 2009; Castillo et al., 2013; Ye et al., 2013). According to the models of Snyder et al. (2002), sea-level drops may form knickpoints if (1) the exposed seafloor (below current sea level) is steeper than the upstream channel (above sea level), (2) the relative rate of base-level change exceeds wave and tide erosion, and (3) the rock-uplift rate remains uniform onshore and offshore. In order to quantify knickpoint propagation rates, it is therefore necessary to identify the initial base level from which the knickpoint started to retreat, which is challenged by the uncertainties on eustasy and vertical motion (Fig. 1A; e.g., Pedoja et al., 2014). Paleo-sea level indicators such as marine terraces (e.g., Castillo et al., 2013) help alleviating these uncertainties.

We focused on an uplifted coastal area characterized by a sequence of emerged coral reef terraces (CRTs) in Sumba Island, Indonesia. CRTs are marine terraces in the broadest sense of the term that thrive in the tropical coastal zones; they include a slightly sloping area separated by steep slopes (Murray-Wallace and Woodroffe, 2014; Pedoja et al., 2018). When relative sea-level drops, the reef emerges, fossilizes, and forms a CRT. The joint effects of sea-level oscillations and tectonic uplift result in the generation of CRT sequences whose staircase geometries are largely structured by sea level highstands (e.g., Chappell, 1974; Pirazzoli, 2005). The CRTs in Sumba Island are worldwide recognized (e.g., Murray-Wallace and Woodroffe, 2014) and associated with an active fringing reef. They are drained by a fluvial system associated with deep canyons. The relative sea level due to Pleistocene glacio-eustatic oscillations, coastal tectonic uplift and the dynamics of the incising channels fingerprints the successive emergences of the coral reef terraces (Nexer et al., 2015, Pedoja et al., 2011; 2014). The major rivers, embedded into the CRT sequence, display pronounced knickpoints (Nexer et al., 2015). At a first order, the longitudinal profile of the rivers mimic the profile of the CRT sequence: the amplitude of knickpoints correlates with the amplitude of the CRT topographic steps.

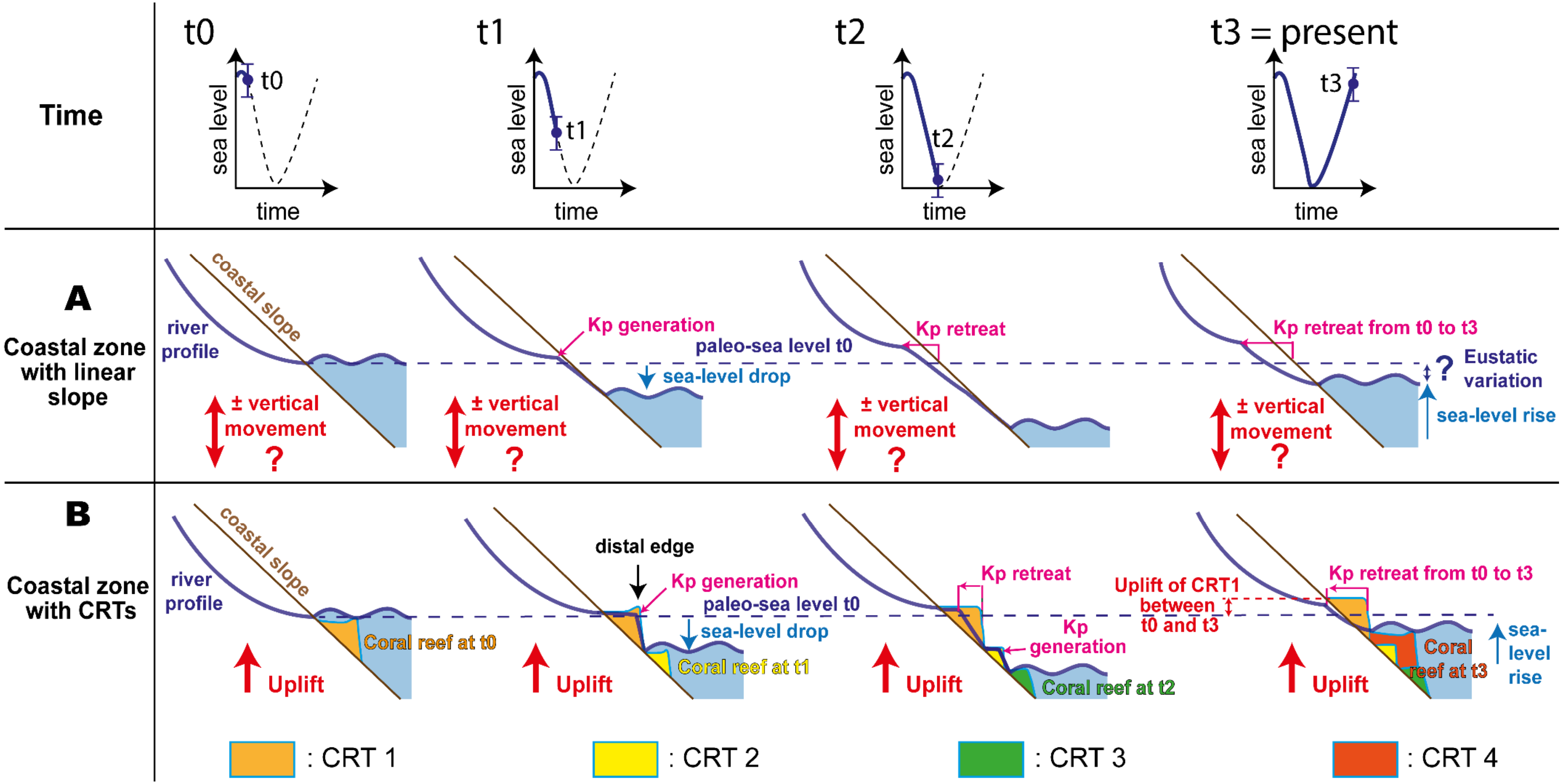

Fig. 1. Eustatic-triggered knickpoint dynamics, in **A)** coastal environment with offshore linear ramp and **B)** coastal zone with emerged coral reef terraces (CRTs), and their association with the distal edge of CRTs.

We thus hypothesize that knickpoints are generated at the distal edge of the CRT, along streams draining an emerged CRT sequence (Fig. 1B). These knickpoints are better expressed than the knickpoints associated with marine terraces because they initially adopt the downstream break in slope of the reef, which is more pronounced than that of a rocky-shore platform from which marine terraces originate (e.g., Castillo et al., 2013). The upstream migration of knickpoints associated with their erosion is produced by the sediment load and the river flow that collectively allow the river to rebalance itself. The distance of a knickpoint from the distal edge of the associated CRT yields the upward retreat length knickpoint migration since the occurrence of the eustatic drop (Figs. 1B; 2). In addition, the coral colonies from a CRT can be dated (e.g., U/Th and ESR-dating; Pirazzoli et al., 1991; Bard et al., 1996), which allows inference of the propagation rates of the knickpoints. Moreover, the propagation rates of active knickpoints can be additionally measured by quantifying denudation rates from terrestrial cosmogenic nuclides (e.g., ^{10}Be or ^{36}Cl) both upstream and downstream of the knickpoint (e.g., Brocard et al., 2016). Finally, the finite eroded volume at the catchment scale can also be determined from the difference between the current topography and the reconstructed surface of the original sequence (Fig. 2; e.g., Molliex et al., 2016). This finite eroded volume at a catchment scale can be compared with denudation rates deduced from terrestrial cosmogenic nuclides measured at the catchment outlet. We applied this multi-method approach with high resolution topographic data (Pleiades imagery) to characterize the dynamics of coastal channels draining the CRT sequence of Sumba Island (Indonesia).

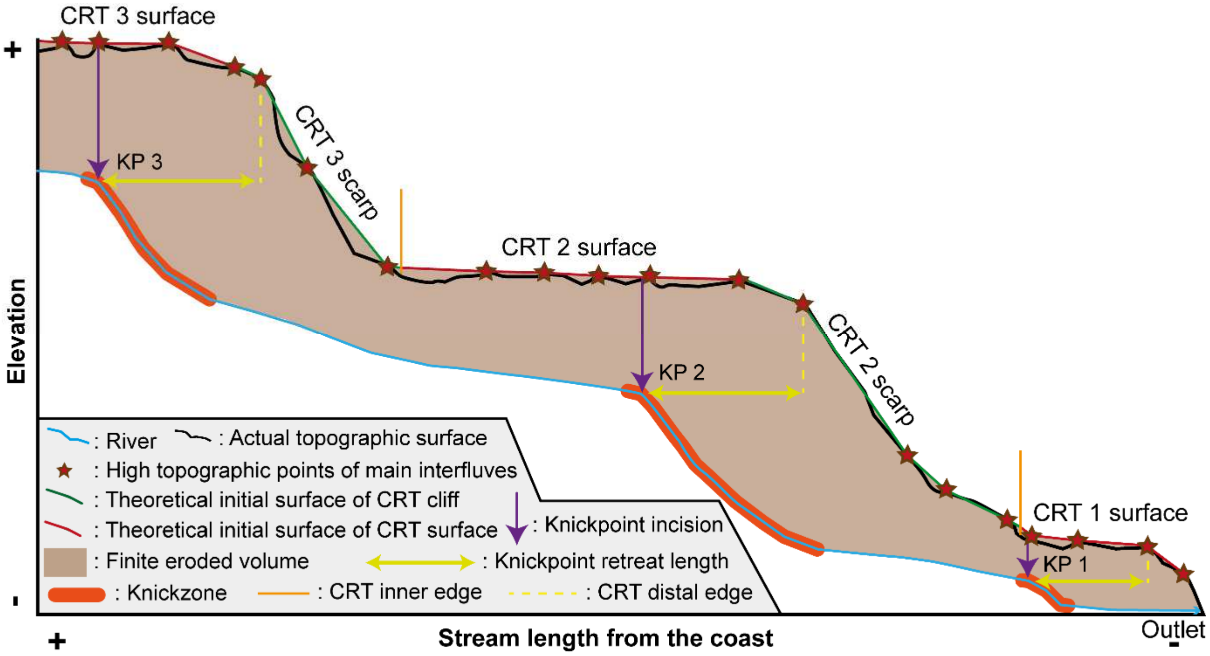

Fig. 2. 2D sketch of a theoretical river draining a CRT sequence, showing the principle of the method of the finite eroded volume calculation (Sections 3.3. and 4.3).

We selected a catchment draining the well-documented coastal sequence of CRTs at Cape Laundi. We detected knickpoints on the longitudinal profile of the main stream, the majority of which are associated with a CRT distal edge, and we calculated knickpoint retreat lengths, finite vertical incision and detrital cosmogenic nuclide ^{36}Cl denudation rates along the channel profile. These data constrain the eustatic knickpoint dynamics at short (10^3 yr, inferred from ^{36}Cl denudation rate), medium (10^4 and 10^5 yr, inferred from knickpoint retreat since a given MIS highstand) and long-term (10^6 yr, inferred from the finite eroded volume of the whole quaternary CRT sequence). We complete the study of the dynamics of coastal transient landscapes by exploring the correlation between catchment-scale denudation rates, finite eroded volume, uplift rate, and catchment drainage area and mean slope. We analyzed the topography of five coastal catchments affected by various uplift rates and quantify ^{36}Cl-derived catchment-scale denudation rates.

2. Settings

Sumba Island is a 220 km-long and 65 km-wide island situated in the Sunda-Banda fore-arc region (Fig. 3).

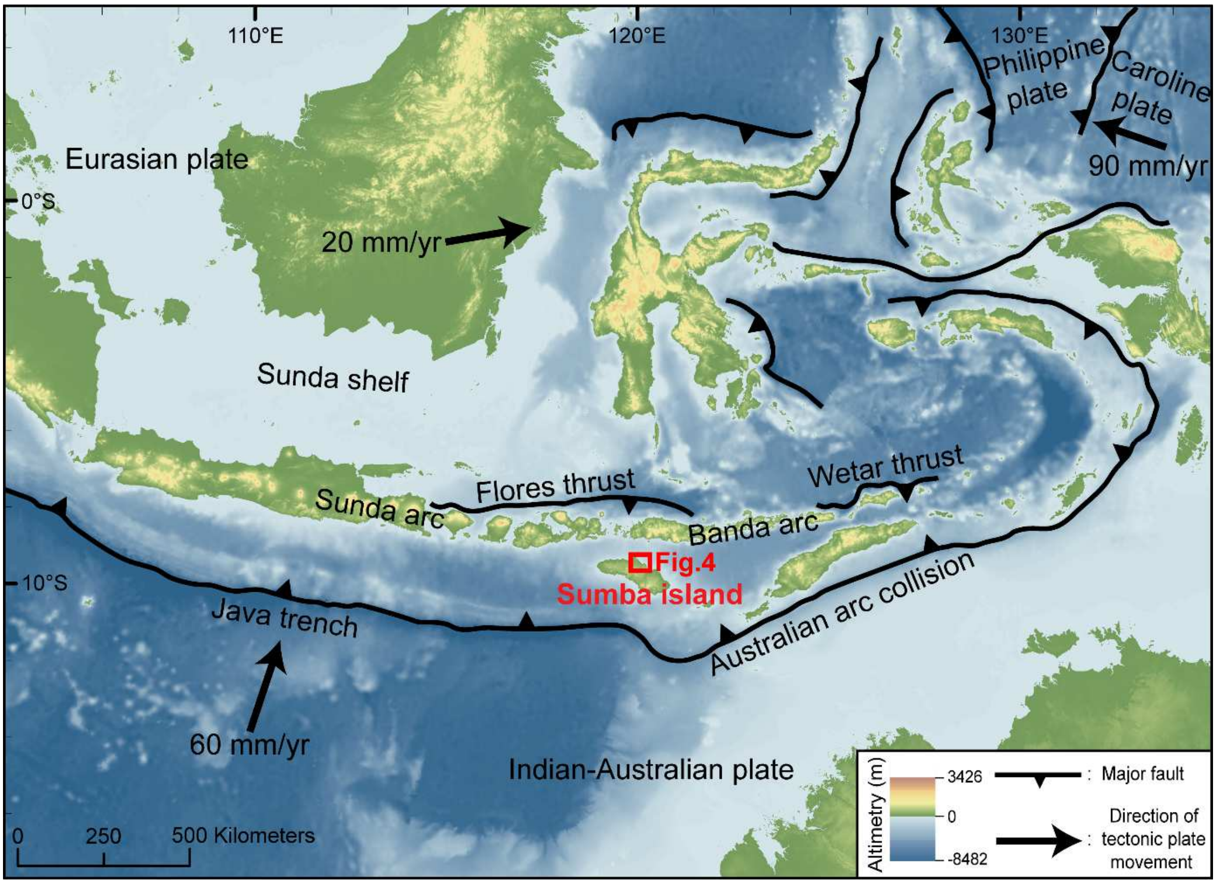

Fig. 3. Geodynamics of SE Asia and location of Sumba Island (Indonesia). Plate velocities indicated with respect to Eurasia plate, from Nugroho et al. (2009), elevation data from the Shuttle Radar Topography Mission (SRTM) and bathymetry data from the General Bathymetric Chart of Oceans (GEBCO).

It lies at the convergent boundary between the Eurasian and Indian-Australian plates. This places it near the transition from oceanic subduction to the West, along the Java trench, to the collision of the Banda arc with the continental Indian-Australian plate to the East (Hinschberger et al., 2005). Sumba Island is the emergent portion of the Sumba Ridge, an isolated tectonic block of crystalline basement located halfway between the Sunda trench and the active volcanic arc (e.g., Fortuin et al., 1997). Subduction of thick buoyant continental Australian crust under the Banda arc started during the Late Miocene and induced uplift and emergence of the Sumba ridge (Harris, 1991; Fortuin et al., 1997; Hall and Smyth, 2008; Haig, 2012). The ensuing uplift is responsible for (1) the diachronic emergence of Sumba starting ~3 Ma ago (Roep and Fortuin, 1996) in the east, and ~1 Ma ago at Cape Laundi (Pirazzoli et al., 1991; 1993; Fig. 4), (2) the formation of an emerged CRT sequence along the northern, western and eastern flanks of the island (Hantoro, 1992; Fleury et al., 2009; Nexer et al., 2015), and (3) coeval south-verging collapse of the southern flank of the island (Fleury et al., 2009). Sumba island consists of Late Cretaceous and Eocene–Oligocene volcanic rocks largely covered by Miocene to Quaternary sediments (Abdullah et al., 2000). The sedimentary cover is composed of the Waikabubak limestones (Mio–Pliocene), Kannanggar limestones and turbiditic sandstones (Mio–Pliocene), and Quaternary reefal limestones (i.e. CRTs) that festoon two thirds of the coastline (Rutherford at al., 2001). The CRT sequence in Cape Laundi develops over the Mio-Pliocene limestones and is incised by linear streams embedded in canyons of decametric depths. These valleys result from tectonic uplift and karstic processes and only seldom reach the Mio/Pliocene basement.

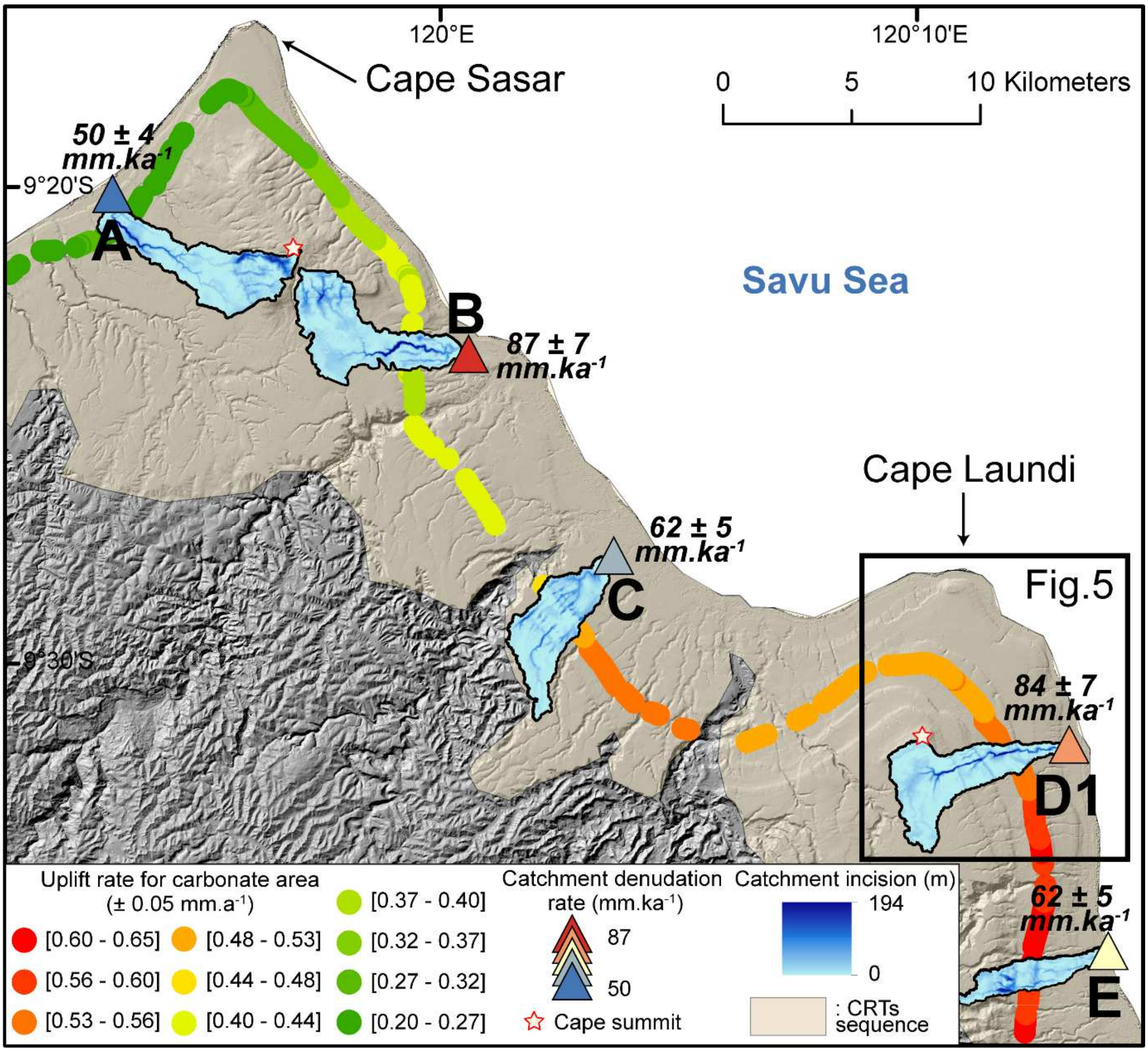

Fig. 4. Map of catchments incision and uplift rates of the studied zone, near Cape Laundi, and location of the sampled catchments. The triangles correspond to the sampling location, and numbering (e.g., D1). Denudation rates, calculated for each catchment outlet, are in bold italics (Table 2).

Detailed studies of the CRT sequences were carried out in our study area at Cape Laundi (Fig. 5). The sequence reaches ~470 m in elevation and has a staircase shape with six main CRTs separated by continuous high (>10 m) fossil sea cliffs (Pirazzoli et al., 1993). Each main CRT includes several intermediate CRTs (Hantoro et al., 1989; Pirazzoli et al., 1993). Based on ~56 ^{230}Th/U-ages, the successive CRTs were correlated to highstands associated with Marine Isotopic Stage (MIS) 1 (~Holocene) to MIS 29 (~1 Ma; Jouannic et al., 1988; Pirazzoli et al., 1991; 1993; Hantoro, 1992; Bard et al., 1996; Chauveau et al., 2021). For the last 600 ka, steady uplift rates are suggested, at 0.49 ± 0.01 mm.a^{-1} (Pirazzoli et al., 1991; 1993) and from 0.20 to 0.50 mm.a^{-1} (Bard et al., 1996). The distal edge of the CRT associated to MIS 11c (i.e. CRT III; Fig. 5), well-marked in the landscape and laterally continuous on all the coastal stretch covered by the CRT sequence of Sumba Island, was used as a morphological benchmark to calculate uplift rate all along the western, eastern and northern coasts of Sumba Island (Nexer et al., 2015). The uplift rates range from 0.02 to 0.06 mm.a^{-1} (Nexer et al., 2015).

Downstream, the active reef contains live coral colonies, which mostly develop on the reef crest and fore reef, with micro-atolls of *Porites* and a few branching corals (Hantoro, 1992). The back reef and reef flat comparatively bear a low density of living corals (i.e. coral cover < 10%) and a coral-algal environment. Most species tolerate episodic emergence and water turbidity (e.g., *Goniastrea retiformis, Acropora digitifera*; Bard et al., 1996).

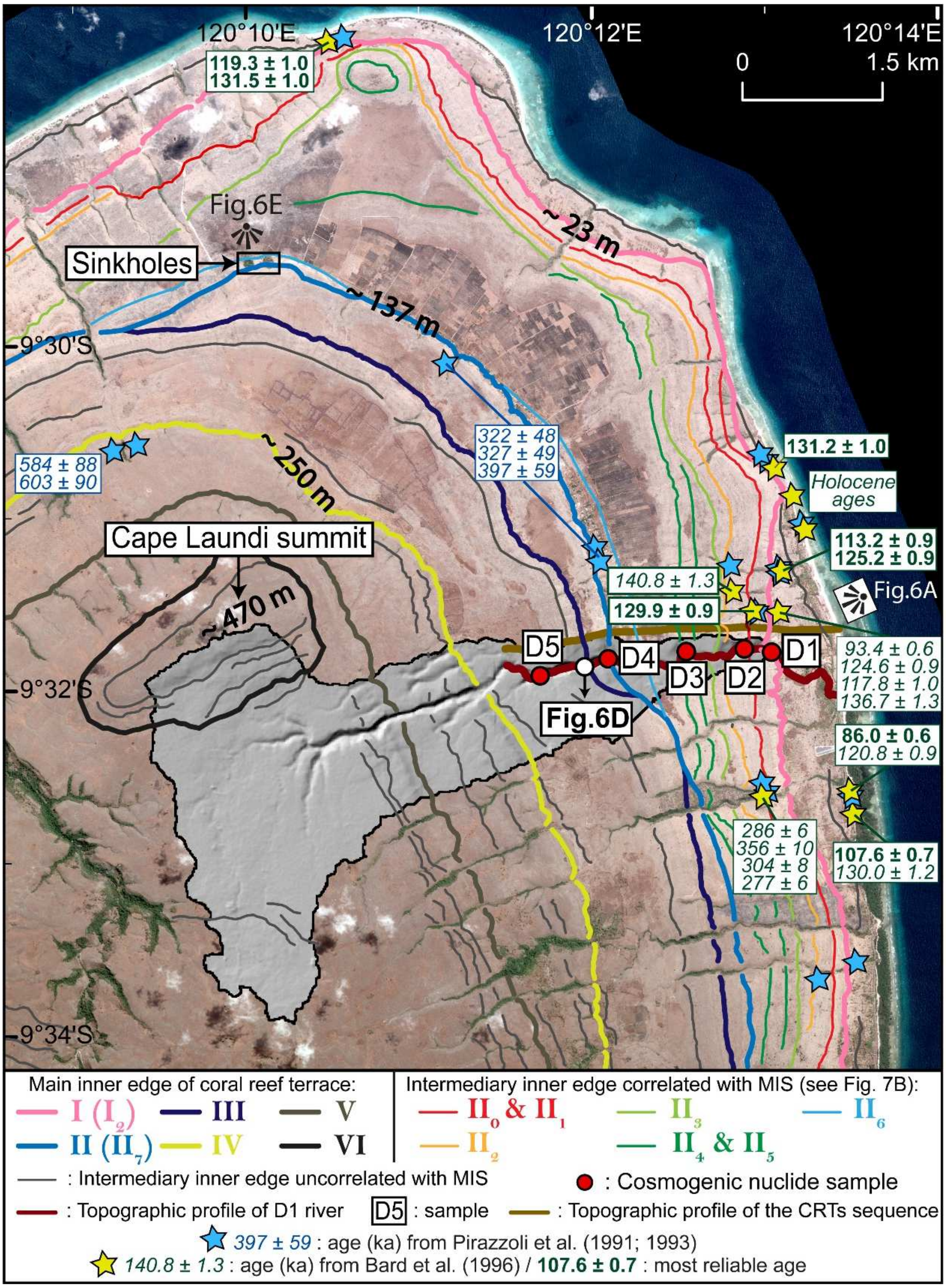

Fig. 5. CRTs at Cape Laundi. The map is drawn on a Pleiades satellite imagery with a 1 m resolution. Location of samples (D2, D3, D4 and D5) and outlet sample (D1) and topographic profiles. Some data from Pirazzoli et al, (1991; 1993) are not located on the map because their coordinates were not provided.

3. Methods

3.1. Quantifications of knickpoint incisions

We selected a coastal channel draining the well documented and dated sequence of Cape Laundi (catchment D1; Figs. 4; 5; Jouannic et al., 1988; Hantoro, 1992; Pirazzoli et al., 1993; Bard et al., 1996; Chauveau et al., 2021) for which we assembled a high-resolution digital elevation model from Pleiades satellite imagery. The stream is embedded in a deep canyon ranging from 0 to 70 m depth. In addition to chemical erosion affecting the CRTs, uplift allows characterizing this canyon as a tectonic gorge. We walked upstream from the sea outlet, following the riverbed to D5 sampling site (Figs. 5; 6A). Beyond this point, the vegetation in the riverbed is too dense to continue. Downstream, the vegetation is concentrated in the lateral slopes of the canyon (Fig. 6A). During our field campaign (July 2018; i.e. during the dry season), the river was dry, which points to an intermittent seasonal cycle (i.e. an activity during the rainy season from November to April; Prasetia et al., 2013; Figs. 6B; 6C; 6D). Yet, the vegetation on the cliff slopes ensures constant humidity in the confined space of the canyon and helps the formation and leaching of soil towards the riverbed, thus supplying sediment load of the catchment. During the rainy season, large blocks detach from the slopes to the riverbed, which increases the (carbonate) sediment load (Fig. 6D).

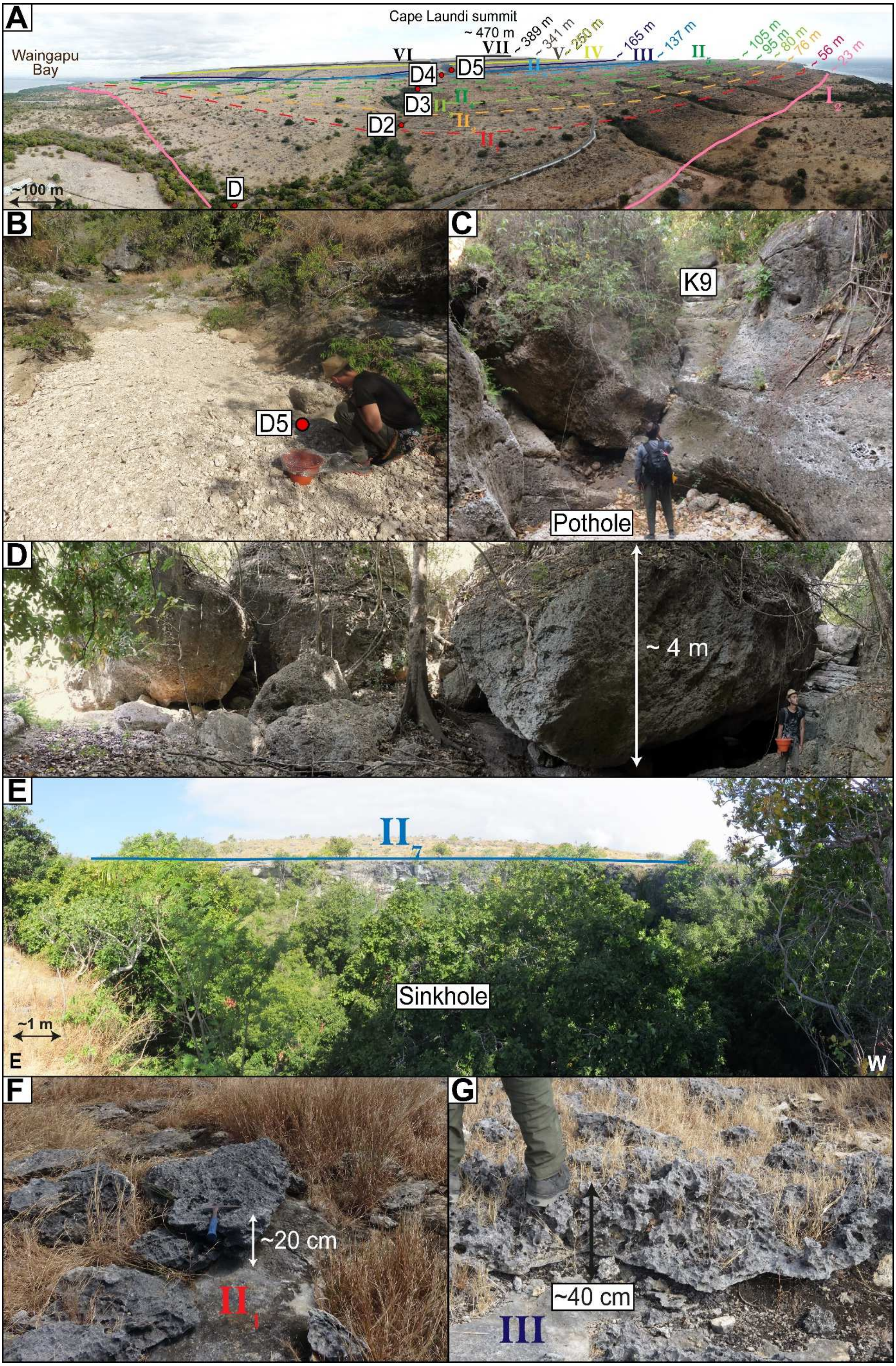
A
Waingapu Bay
Cape Laundi summit
~ 470 m
VI
VII
~ 389 m
~ 341 m
V
~ 250 m
IV
~ 165 m
III
~ 137 m
II_7
II_5
~ 105 m
~ 95 m
~ 80 m
~ 76 m
~ 56 m
~ 23 m
I_2
D5
D4
D3
D2
II_4
II_3
II_2
II_1
~100 m
D
B
D5
C
K9
Pothole
D
~ 4 m
E
II_7
Sinkhole
~1 m
E
W
F
~20 cm
II_1
G
~40 cm
III

Fig. 6. Interpreted pictures of the Cap Laundi emerged CRT sequence and the canyon draining them (catchment D1). **A)** Aerial photo of Cape Laundi showing the staircase coastal landscape (location of capture on Fig. 5). **B)** Sampling site of sample D5. **C)** Knickpoint K9 (see location on Fig. 7B). **D)** Collapsed blocks in the canyon (location on Fig. 5). **E)** Sinkhole of Cape Laundi (location on Fig. 5). Epikarst on the surface of CRT **F)** II_1 and **G)** III.

River D1 displays pronounced knickzones that are commonly located by waterfalls that incise the CRTs, sometimes carving potholes (Fig. 6C). These river segments are free of sediments. We mapped all the knickzones along the selected coastal stream from field observations, GPS and DGPS data and satellite imagery (Pleiades). We identified each eustatic knickpoint that could be associated with the distal edge of a CRT (Fig. 1B). To properly correlate a knickpoint to the CRT distal edge, and therefore to the MIS responsible for the formation of the CRT, we considered that the knickpoint must be 1) located upstream from the CRT distal edge, and 2) topographically lower than the distal edge of the CRT. Above and below the knickpoints, the bedrock is homogeneous and partly covered by sediments (Fig. 6B). Carbonated sands and gravels are abundant enough to allow sampling for ^{36}Cl cosmogenic nuclide analysis, on both sides of knickpoint, where the stream slope is lower (i.e. sampling areas; Fig. 6B).

We calculated the steepness index for each 100-m-long river segment of D1 channel (e.g., Wobus et al., 2006; Kirby and Whipple, 2012; Castillo et al., 2014). Under steady state conditions, fluvial channels can be conveniently reconstructed using a power-law relationship (Flint, 1974):

$$S = k_s\, a^{-\theta}, \tag{1}$$

where k_s is the steepness index, S is the slope, a is the upstream catchment area, and θ is the concavity index. Because concavity varies among rivers and that variation leads to large changes in k_s, the steepness index is often expressed in a normalized form, k_{sn}, by using the same reference concavity, θ_{ref}, for all channels being analyzed (e.g., Snyder et al., 2000; Duvall et al., 2004; Kirby and Whipple, 2012), such that:

$$S = k_{sn}\, a^{-(\theta_{ref})}, \tag{2}$$

where $\theta_{ref} = 0.45$ is a standard value in the literature. k_{sn} values increase drastically downstream knickpoints.

The mobility of knickpoints can be inferred from a slope-area relationship (Kirby and Whipple, 2012). Vertical-step knickpoints are stationary and reveal discrete heterogeneities whereas knickpoints that represent a break in slope-area scaling typically develop in response to a persistent change in forcing, either spatial or temporal (Kirby and Whipple, 2012).

3.2. Denudation rate inferred from terrestrial Cosmogenic Nuclide ^{36}Cl Concentration (CNC)

To examine the relationships between denudation rates, uplift rate and catchment metrics, we selected five catchments in the same area along the central part of the northern coast of Sumba. They collectively only drain the CRT sequence, but uplift at variable rates (from 0.2 to 0.6 mm.a^{-1}; Fig. 4). We sampled sands at river outlets to measure the ^{36}Cl cosmogenic nuclide concentration. To evaluate the spatial variations of denudation rate along a coastal channel due to its transient state, we sampled at five sites separated from one another by knickpoints (catchment D1; Fig. 5).

Cosmogenic nuclide ^{36}Cl is appropriate for reefal limestones. Carbonate rocks accumulate ^{36}Cl cosmogenic nuclides over the uppermost meters of soil because of the interactions of Ca with secondary cosmic rays (e.g., Stone et al., 1994). After some exposure, ^{36}Cl concentration will rise and plateau to value determined by the trade-off between ^{36}Cl production rate and surface denudation rate (Bierman, 1994). ^{36}Cl concentration is inversely proportional to the surface denudation rate (e.g., Granger and Riebe, 2014). ^{36}Cl concentrations of river sediments thus scale with average denudation rate over the catchment (Brown et al., 1995; Bierman and Steig, 1996; Granger et al., 1996). The time scales over which denudation rates are averaged are inversely proportional to denudation rate and is approximately equivalent to the time required to remove ~60 cm of bedrock (von Blanckenburg, 2005).

We used a standard chlorine extraction technique with leaching to eliminate any potential meteoric ^{36}Cl (Stone et al., 1996; Merchel et al., 2008; Schlagenhauf et al., 2010). Each sample was washed and the fraction 250-1000 µm extracted. About ~100 g of each sample is used for chemical analysis. Major oxides (SiO_2, TiO_2, Al2O_3, Fe_2O_3, MnO, MgO, CaO, Na_2O, K_2O, P_2O_5) and trace elements (Li, Be, Mo, Ba, Sm, Gd, Pb, Th, U, Sc, Cr, Cr, Co, Ni, Rb, Sr) have been measured on bulk samples (i.e. the fraction finer than 250 µm collected after crushing), respectively by an ICP AES - Ultima 2 - Jobin Yvon and a HR-ICP-MS Element XR, at the LGO (Laboratoire Géosciences Océan, IUEM) in Brest (France). CO_2 concentration is determined by weighing the samples, dissolving them in a Gas Bench and measuring the CO_2 produced (Pôle de Spectrométrie Océan, Plateforme Isotopes Stables, IUEM, Brest, France). Cl isotopic ratio was measured by Accelerator Mass Spectrometry (AMS) at CEREGE (Centre de Recherche et d'Enseignement de Géosciences de l'Environnement) in Aix-en-Provence (France). Analytical uncertainties include uncertainties associated with AMS counting statistics, chemical blank measurements, and AMS internal error (0.5%). ^{36}Cl production and denudation rates were calculated following Schimmelpfennig et al. (2009) taking into account sea-level and high-latitude production rates for rapid neutron spallation reactions in Ca (42.2 ± 2 atoms ^{36}Cl (g Ca^{-1} a^{-1}); Braucher et al., 2011; Schimmelpfennig et al., 2011; 2014), negative muons (Heisinger et al, 2002), rate of epithermal neutron production from fast neutrons (Phillips et al., 2001) and production from radiogenic neutrons (Fabryka-Martin, 1988; Phillips and Plummer, 1996; more information related to ^{36}Cl production is detailed in Appendix "A" of Schimmelpfennig et al., 2009). The effective fast neutron attenuation coefficient is 177 ± 4 $g.cm^{-2}$ (Farber et al., 2008). Topographic shielding was calculated for each sample (i.e. average over the whole catchment) using the topographic shielding add-in for ArcGIS software (Codilean, 2006). The scaling factors for nucleonic and muonic production are calculated with CosmoCalc 1.7 macro (Vermeesch, 2007; Dunai, 2010) and with the mean elevation, longitude and latitude of each catchment.

The uncertainty on the extent of the actual catchment area contributing to stream sediments adds to the uncertainty of the measured ^{36}Cl concentrations. The sub-horizontal parts of the catchment area (i.e. the CRT surfaces) will mainly be affected by chemical erosion, by means of sinkholes and epikarsts (Figs. 5; 6E; 6F; 6G; e.g., Authemayou et al., 2018; Chauveau et al., 2021). Consequently, it is difficult to quantify dissolution inputs to karst surfaces and thus catchment parts that do not significantly contribute to canyon inputs. To overcome this problem, we assume that the overwhelming majority of the sediment supply comes from the canyon area itself, that we define as a valley wherein slopes are systematically greater than ~10°. To obtain the maximum and minimum limits of the sediment supply area, we calculated the denudation rates both for the whole drainage area extracted automatically with the Digital Elevation Model (DEM), and for the canyon area only.

3.3. Catchment metric and finite eroded volume of the emerged coral reef terrace sequence

Morphometric parameters were computed for each catchment from the 12 m TanDEM-X (the elevations are converted to orthometric heights; Boulton and Stokes, 2018) using Rivertools (http://rivix.com/) to determine if the catchment denudation rate is a function of internal parameters. We extracted for each catchment the drainage area (catchment versus canyon), the finite eroded volume and the mean slope of the canyon. In view of the particular morphology drained by the catchments, it is necessary to also focus on the catchment metric parameters and finite eroded volume restricted to the canyon areas that concentrate most of the mechanical erosion.

We calculated the uplift rates using the present-day elevation of the CRT III distal edge (± 2 m at Cap Laundi, and ± 12 m on the rest of the island), correcting for eustasy, during MIS 11c (-1.5 ± 11 APSL; Bowen, 2010), and assigning an age of 390 ± 20 ka to MIS 11c (Murray-Wallace and Woodroffe, 2014). We attribute a mean uplift rate to each catchment with the uplift rate values calculated along the MIS 11 CRT segment located on their drainage area.

To assess the lateral continuity of the CRT sequence, we also make use of stacked swath profiles (Armijo et al., 2015; Fernández-Blanco et al., 2019). These are constructed using a large number of parallel swath profiles (here 600) to derive a 2.5-D view of the landscape. Areas of the overall morphology with several lines stacked together denote relatively flat surfaces separated by more or less steep slopes; in this case, the CRTs of the sequence.

Long-term denudation estimates from finite eroded volume were obtained by subtracting the actual topography (TanDEM-X and Pleiades imagery DEM) from a reconstructed topography that attempts to compensate the effects of erosion. We computed this theoretical uneroded surface from envelope of the highest points of the sequence, after extraction of high points and main interfluves from the DEM, using the “Topo to Raster” tool in “Spatial Analyst” extension of ArcGis software (e.g., Small and Anderson, 1998; Molliex et al., 2016; Fig. 2). This tool interpolates the elevation values of a raster by imposing constraints to ensure a drainage structure that is connected and the correct representation of ridges and streams from the input isoline data. The volume yielded by such an approach requires a subjective adjustment, for it relies on the number of control points selected to reconstruct the purportedly pristine topography (Lucazeau and Hurtrez, 1997; Champagnac et al., 2012). If such points are too sparse, some reliefs may not be taken into account and the interpolated envelope can locally be lower in elevation than the actual topography. On the contrary, oversampling the topography yields an interpolated envelope that is close to present-day topography. The difference between present-day topography elevation and the reconstructed surface yields the minimum finite eroded volume by coastal channels, since CRT distal edges experienced in-situ denudation (Chauveau et al., 2021). In this study, because of the staircase morphology of the sequence, with a fossil sea cliff separating successive CRTs, the finite eroded volumes are first calculated for the main surfaces of the CRT and then for the cliffs between two CRTs (Fig. 2). We assumed that the total finite eroded volume yielded by such a method globally represents the finite eroded volume of coastal drainage since the beginning of the incision following the emergence of the oldest CRT giving a mean long-term denudation rate of ~1 Ma at Cape Laundi (Pirazzoli et al., 1991). We also used this method to calculate the maximum vertical incision of the knickpoint and the vertical incision all along the stream profile of catchment D1 (Fig. 2).

4. Results

4.1. Catchment D1: Morphological characteristics and knickpoints

Catchment D1 is small (10.9 km^2; Table 1) and its main stream (~7.6 km) is almost linear and deeply incises the CRT sequence in a canyon (Figs. 5; 6A; 7; 8A). Except within the canyon, the staircase morphology of the CRT sequence is well preserved. The drainage area restricted to the canyon is 1.2 km^2 (Table 1).

Catchment name	Mean elevation (m)	Catchment area (km^2)	Canyon area (km^2)	Uplift rate (mm a^{-1})	Mean slope of canyon area (°)	Finite eroded volume of catchment (km^3; ± 1.10^{-6})	Finite eroded volume of canyon area (km^3; ± 1.10^{-5})
A	196	11.8	1.5	0.27 ± 0.03	15.3	0.0638	0.0271
B	220	12.2	3.9	0.39 ± 0.03	12.3	0.0699	0.0505
C	216	9.5	1.7	0.45 ± 0.04	10.6	0.0434	0.0199
D1	343	10.9	1.2	0.51 ± 0.04	17.9	0.0434	0.0209
E	239	4.4	1.3	0.61 ± 0.04	13.4	0.0264	0.0152

401 **Table 1.** Synthesis of metrics from studied catchments in Sumba Island.

We identified 14 knickpoints along the stream profile from the outlet up to 4 km upstream (Figs. 7; 8B; 8C). The majority of these knickpoints are also highlighted by higher steepness index (i.e. k_{sn}) values downstream than upstream (Fig. 8C). Nine of them have been correlated with distal edges of CRTs and assigned to sea level highstands (Figs. 7A; 7B; Pirazzoli et al., 1991; 1993; Bard et al., 1996). More specifically, K2, K4, K6, K7/K8, K9, K10, K11, and K12 are respectively associated with regressions following MIS 5e, MIS 7a, MIS 7c, MIS 7e, MIS 9a, MIS 9c, MIS 9e and MIS 11c highstands (Figs. 7A; 7B). Their retreat lengths range from 209 to 376 m (Figs. 7B). Five small knickpoints could not be correlated to any CRT (K1, K3, K5, K12 and K14; Fig. 7B).

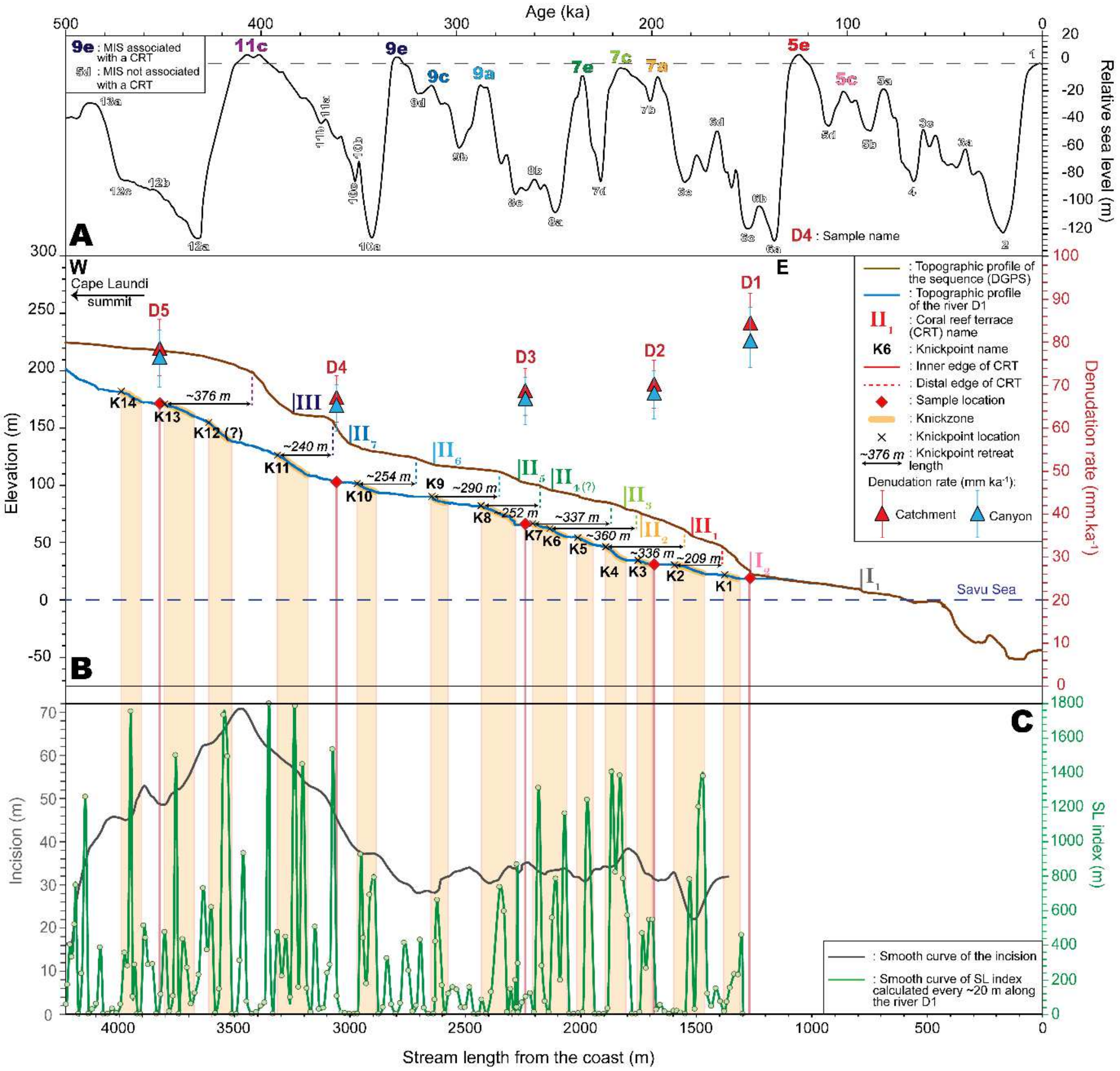

Fig. 7. The knickpoints of the Cape Laundi river. **A)** Relative sea level curve from Waelbroeck et al. (2002). **B)** Elevation profiles (derived from Pleiades DEM and GPS measurement) of the Cape Laundi main river (catchment D1) and associated profile of the emerged CRT sequence, in relation with the calculated cosmogenic ^{36}Cl denudation rates with catchment areas extracted from DEM (red triangles) and with canyon areas (blue triangles), as well as the location of knickzones (orange areas), distal edge of CRT and knickpoint retreat length. **C)** Incision (black line) and SL index (green line and marks) along the stream profile.

4.2. Denudation rates inferred from Cosmogenic Nuclide ^{36}Cl Concentration (CNC)

Catchment denudation rates calculated for the five selected catchments (Fig. 4) range from 50 ± 4 mm.ka^{-1} (sample A) to 87 ± 7 mm.ka^{-1} (sample B) with an average of 69 ± 8 mm.ka^{-1} (n = 5;Table 2). Catchment denudation rates calculated for the canyon area range from 49 ± 4 mm.ka^{-1} (sample A) to 87 ± 7 mm.ka^{-1} (sample B) with an average of 68 ± 8 mm.ka^{-1} (n = 5; Table 2). Along the river of catchment D1, denudation rates range from 69 ± 5 mm.ka^{-1} (sample D4) to 78 ± 7 mm.ka^{-1} (sample D1) with an average of 71 ± 5 mm.ka^{-1} (n = 5; Table 2; Fig. 7B). Samples D4, D3, D2 present comparable low values, whereas D5 and D1 have the highest denudation rate values (Table 2; Fig. 7B). In this study, the calculated integration times of denudation rates range from 6.9 ± 0.5 ka (highest denudation rates; sample B) to 12.0 ± 0.8 ka (lowest denudation rates; sample A), with an average of 8.8 ± 1.6 ka (n = 5; Table 2).

Sample	Information	Longitude	Latitude	Elevation	N_{meas}	$S_{el,s}$, $S_{el,n}$	$S_{el,\mu}$	P_s	P_{eth}	P_{th}	P_μ	P_r	Denudation rate of whole catchment	Denudation rate of canyon	Integration time
		(E)	(N)	(m)	(10^5 atom g^{-1} rock)	(± 0.04)	(± 0.03)	($g(^{36}Cl)^{-1}yr^{-1}$)	($g(^{36}Cl)^{-1}yr^{-1}$; ± 0.01)	($g(^{36}Cl)^{-1}yr^{-1}$; ± 0.02)	($g(^{36}Cl)^{-1}yr^{-1}$)	($g(^{36}Cl)^{-1}yr^{-1}$)	(mm ka^{-1})	(mm ka^{-1})	ka
A	drains only carbonate surfaces	119.88	-9.34	10.3	4.39 ± 0.10	0.68	0.65	19.60 ± 0.81	0.09	0.24	3.65 ± 0.91	0.0031	50.1 ± 4.2	49.4 ± 4.2	12.0 ± 0.8
B		120.01	-9.39	12.2	2.35 ± 0.05	0.70	0.65	18.58 ± 0.77	0.04	0.11	3.31 ± 0.83	0.0013	87.0 ± 7.2	86.8 ± 7.2	6.9 ± 0.5
C		120.06	-9.45	12.5	3.72 ± 0.08	0.69	0.65	19.62 ± 0.81	0.07	0.19	3.81 ± 0.95	0.0020	61.5 ± 5.3	60.6 ± 5.2	9.8 ± 0.7
D1		120.01	-9.39	25.4	2.77 ± 0.06	0.76	0.69	19.02 ± 0.79	0.10	0.33	3.49 ± 0.87	0.0033	84.2 ± 7.0	81.3 ± 6.8	7.1 ± 0.5
E		120.23	-9.60	6.0	3.23 ± 0.07	0.71	0.66	18.69 ± 0.77	0.05	0.16	3.09 ± 0.77	0.0014	61.7 ± 5.0	62.4 ± 5.0	9.7 ± 0.7
D2	Knickpoints (catchment D)	120.21	-9.53	30.6	2.91 ± 0.06	0.77	0.69	18.05 ± 0.75	0.08	0.25	2.97 ± 0.74	0.0030	70.3 ± 5.6	68.2 ± 5.4	8.5 ± 0.6
D3		120.21	-9.53	65.2	3.12 ± 0.07	0.77	0.70		0.09	0.28	3.09 ± 0.77	0.0036	68.8 ± 5.4	66.9 ± 5.3	8.7 ± 0.6
D4		120.20	-9.53	103.6	3.19 ± 0.07	0.78	0.70	18.10 ± 0.75	0.09	0.25	3.12 ± 0.78	0.0036	67.3 ± 5.4	65.4 ± 5.3	8.9 ± 0.6
D5		120.20	-9.53	200.3	3.07 ± 0.07	0.79	0.71	19.20 ± 0.79	0.06	0.17	3.62 ± 0.90	0.0024	78.4 ± 6.6	76.5 ± 6.4	7.7 ± 0.5

Table 2. ^{36}Cl concentrations in present-day river sands sampled at catchments outlets, the scaling factor for nucleonic ($S_{el,s}$-$S_{el,n}$) and muonic ($S_{el,\mu}$) production, ^{36}Cl production rate by spallation of target elements (P_s), capture of epithermal neutrons (P_{eth}), capture of thermal neutrons (P_{th}), capture of slow negative muons (P_μ), radiogenic ^{36}Cl production rate (P_r) and derived denudation rates.

4.3. Finite eroded volume and vertical incision

The finite eroded volumes calculated for the five selected catchments range from ~0.026 km^3 (sample E) to ~0.070 (sample B) km^3 with an average of 0.049 ± 0.017 km^3 (Table 1). The finite eroded volumes values restricted to canyon range from ~0.015 (sample E) to ~0.050 (sample B) km^3 with an average of 0.027 ± 0.013 km^3 (Table 1). Therefore, canyons are responsible for ~53 % of the finite eroded volume in average, ranging from ~42 % (catchment A) to ~72 % (catchment B).

Incision along stream D through the canyon is up to 70 m between knickpoints K14 and K10 through CRT older than MIS 9e (Fig. 7B). Maximum incision is found at the distal edge of the CRT associated with the MIS 11c highstand (Fig. 7B). Down-stream, incision values are comparable (~35 m) and decrease downstream of the distal edge of the MIS 5e CRT to a few meters (Fig. 7B).

4.4. Morphological and environmental parameters of catchments

Morphometric parameters computed for the five catchments are summarized in Table 1. Uncertainties in the averages correspond to standard deviations. The drainage areas of the catchments range from 4.40 km^2 (catchment E) to 12.23 km^2 (catchment B), with an average of 9.75 ± 1.60 km^2. The area of the canyon covers a minimum of 1.17 km^2 (catchment D1) and reaches a maximum of 3.85 km^2 (catchment B). The mean slope of the catchment ranges from 5.54° (catchment C) to 8.26° (catchment E), and averages to 6.59 ± 1.05°. The mean slope restricted to canyons ranges from 10.58° (catchment C) to 17.92° (catchment D1), and averages to 13.90 ± 1.41°. The uplift rates range from 0.27 ± 0.02 mm.a^{-1} (catchment A; Cape Sasar) to 0.60 ± 0.03

mm.a^{-1} (catchment E; North of Waingapu Bay), with an average of 0.45 ± 0.12 mm.a^{-1} (Table 1; Nexer et al., 2015).

5. Discussion

5.1. Eustatic knickpoints on coral reef terraces sequence

5.1.1. Making the case for eustatic knickpoints

Our findings indicate that the majority of the Cape Laundi knickpoints are transient eustatic knickpoints (9 out 14 knickpoints). First, the knickpoints are easily associated with a CRT distal edge from the geomorphologic profiles, i.e. their point of origin during the emergence of the CRT and the beginning of their subaerial incision can be easily identified (Figs. 1B; 7B). Then, at the scale of catchment D1, the uplift rate is spatially uniform (no lateral variability in the elevation of the inner edge of each CRT in the catchment area; Fig. 8E) and temporally constant (Pirazzoli et al., 1991; 1993; Nexer et al., 2015). There is no morphological evidence of active faulting (i.e. no linear fault scarp was detected on the CRTs' surface), which may rule out the possibility of tectonic knickpoints. The seismicity of the subduction zone on Sumba Island is moderate (e.g., Jones et al., 2014), where no historical earthquakes have produced coastal uplift on the island, and no co-seismic terraces have been observed at Cape Laundi. Therefore, it is unlikely that knickpoints (K1, K3, K5, K12 and K14) are associated with co-seismic terrace formation. Furthermore, over the studied area, the lithology is uniform, i.e. exclusively composed of reef limestones, ruling out lithological knickpoints. Also, the catchments are too small to have a significant climatic gradient within the catchment, excluding climatic influence on knickpoint development. Finally, the three conditions that lead to the formation of eustatic knickpoint (following Snyder et al., 2002) are reached: 1) eustatic knickpoints are caused by the emergence of the fore-reef steeper than the upstream channel; 2) wave-base erosion has not balanced the uplift rate otherwise the sequence could not be built; and 3) there are no spatial variations in uplift rates onshore and offshore since the coast is normal to the regional tectonic tilting axis (Nexer et al., 2015).

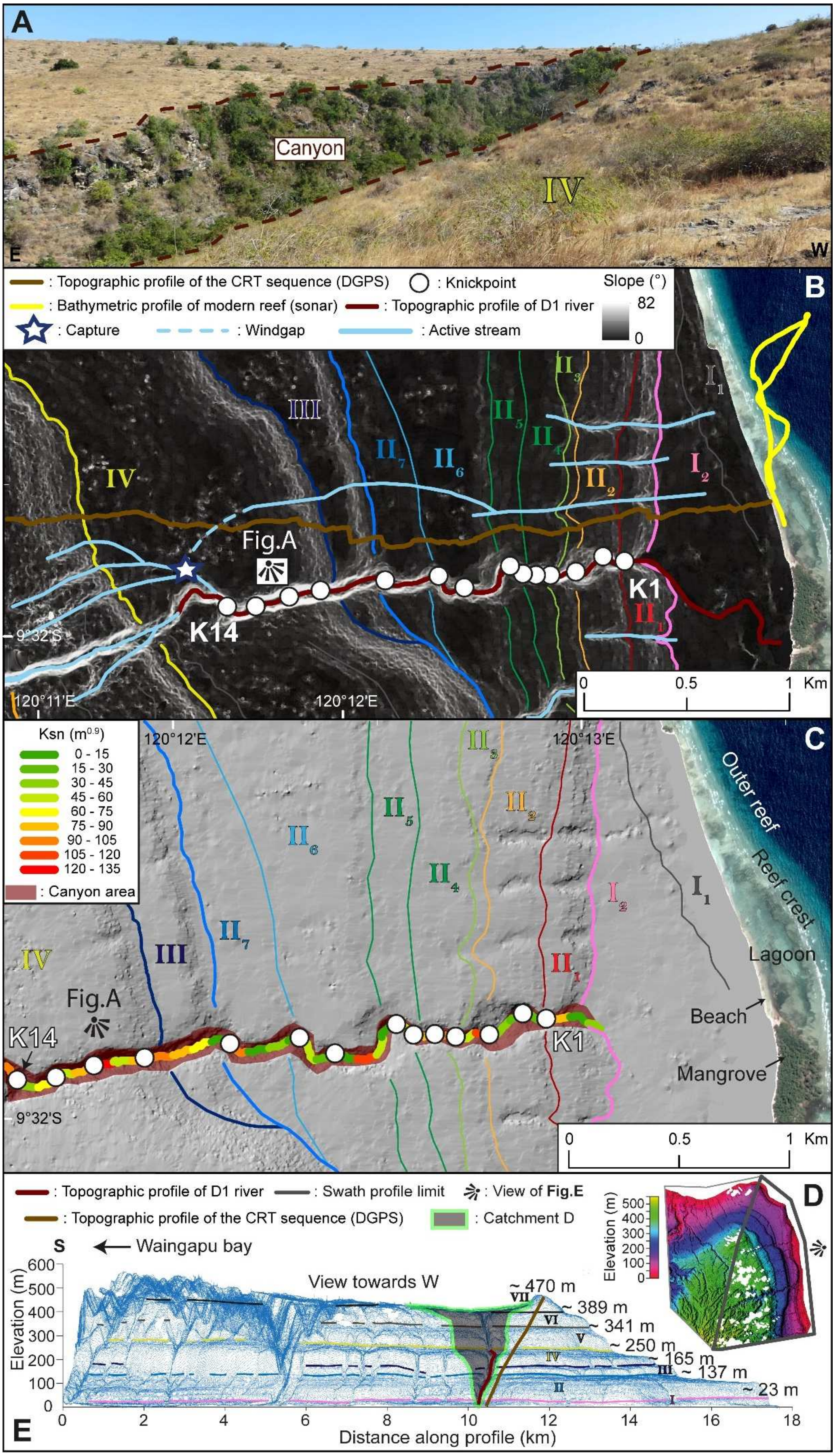
A
Canyon
IV
E
W
: Topographic profile of the CRT sequence (DGPS)
: Knickpoint
Slope (°)
82
0
: Bathymetric profile of modern reef (sonar)
: Topographic profile of D1 river
: Capture
: Windgap
: Active stream
B
IV
III
II7
II6
II5
II4
II3
II2
I1
I2
II1
Fig.A
K14
K1
9°32'S
120°11'E
120°12'E
0
0.5
1 Km
Ksn (m0.9)
0 - 15
15 - 30
30 - 45
45 - 60
60 - 75
75 - 90
90 - 105
105 - 120
120 - 135
: Canyon area
120°12'E
120°13'E
C
Outer reef
Reef crest
Lagoon
Beach
Mangrove
IV
III
II7
II6
II5
II4
II3
II2
II1
I2
I1
Fig.A
K14
K1
9°32'S
0
0.5
1 Km
: Topographic profile of D1 river
: Swath profile limit
: View of Fig.E
: Topographic profile of the CRT sequence (DGPS)
: Catchment D
D
Elevation (m)
500
400
300
200
100
0
S
Waingapu bay
View towards W
~ 470 m
~ 389 m
~ 341 m
~ 250 m
~ 165 m
~ 137 m
~ 23 m
VII
VI
V
IV
III
II
I
Elevation (m)
600
500
400
300
200
100
0
0
2
4
6
8
10
12
14
16
18
Distance along profile (km)
E

Fig. 8. A) Canyon in catchment D1. **B)** Slope map of the south-east of Cape Laundi, showing the different altimetric profiles (bathymetric and topographic), the location of the knickpoints and the inner edge of the low CRTs. **C)** Hillshade map of the Digital Elevation Model (2 m in resolution) based on Pleiades images southeast of Cape Laundi, showing the canyon area, steepness index values (i.e. k_{sn}) along river D1, knickpoint locations, inner edges of low CRTs, and current coastal morphology (beach, mangrove, fringing reef). **D)** Hillshaded Digital Elevation Model (2 m in resolution) from Pleiades images. The white spots inside the hillshade correspond to the clouds in the Pleiades images. **E)** Stacked swath profiles (600 profiles, vertical exaggeration x6, viewpoint location in panel D) and main inner edges of the CRT sequence at Cape Laundi.

Five knickpoints of lower amplitude (i.e. the height between the bottom and the top of the knickzone) are not correlated to a CRT (K1, K3, K5, K12, K14). K1 is located just downstream of K2, which was correlated to the post-MIS 5e regression. The CRT associated with MIS 5c does not exhibit a clear distal edge that could be correlated with K1 (Fig. 7B). This CRT was reworked by marine erosion during MIS 5a and Mid-Holocene highstand (Chauveau et al., 2021). Consequently, the distal edge of the MIS 5c CRT has been eroded, excluding a direct correlation of K1 to this CRT. Other explanations can be proposed related to eustatic forcings for K5, K3 and K1. During regression, when sea level reached a lower elevation than the distal part of the newly emerged CRT, an acceleration of the base-level drop could generate a second knickpoint (Cantelli and Muto, 2014). For instance, K5, K3 and K1 are located downstream of a large knickzone probably related to the onset of a major regression (Fig. 7B). Thus, they could have been produced during the sea-level drop. Cantelli and

Muto (2014) demonstrate that a single perturbation of base level (e.g., eustatic drop) can generate multiple knickpoints. Therefore, it cannot be excluded that several knickpoints are associated with the same regressive event. Knickpoints could also be produced by a sudden sediment supply locally triggered by landslides on incised stream sides, river captures, or confluences. Confluences may suddenly increase the runoff and sediment supply of the main stream and could thus impact its longitudinal profile (Hayakawa and Matsukura, 2003; Crosby and Whipple, 2006). The location of K14 in the upstream part of the stream profile D at a confluence (Fig. 8B) could explain their formation. Yet, river capture cannot be excluded too, because an inactive secondary pathway to the tributary located in the flat part of CRT IV, upstream of the confluence (Fig. 8B).

5.1.2. Dynamics of eustatic knickpoints

Comparing river profiles with the coastal sequence topographic profiles, we observed that eustatic knickpoints are lower in elevation than their associated CRT distal edges, and the morphology of knickpoints is smoother than the staircase shape of the sequence (Fig. 7B). More precisely, the initial steep segment downstream of the knickpoint decreased in slope by rotation of the segment at the base of the knickzone (Gardner, 1983). These observations indicate that these knickpoints have propagated upward with vertical incision and a rotation mode (Gardner, 1983; Castillo et al., 2013). If the erosive efficiency was constant along the stream and if knickpoint retreat was steadily active, an upstream increase in knickpoint retreat length and an upstream decrease in knickpoint amplitude would be observed (Gardner, 1983; Schumm, 1993; Snyder et al., 2002; Whipple and Tucker, 2002; Loget and Van Den

Driessche, 2009). However, our results show that the knickpoint retreat length does not increase upstream (Fig. 7B). The knickpoint retreat lengths are comparable (from 209 m to 376 m) and knickpoint morphologies remain preserved, even the earliest ones (300 to 400 ka ago, K11, K13). Furthermore, no relationship can be noticed between the knickpoint retreat lengths and their assumed age ($R^2 = 0.08$; Fig. 10A). It suggests that knickpoint retreats ceased before their full propagation. In addition, the slope-area scaling relationships of the D1 channel (Figs. 9A; 9B) displays a vertical-step knickpoint form, despite the small spacing between each knickpoints, indicative of stationary knickpoints (e.g., Korup et al., 2010; Kirby and Whipple; 2012).

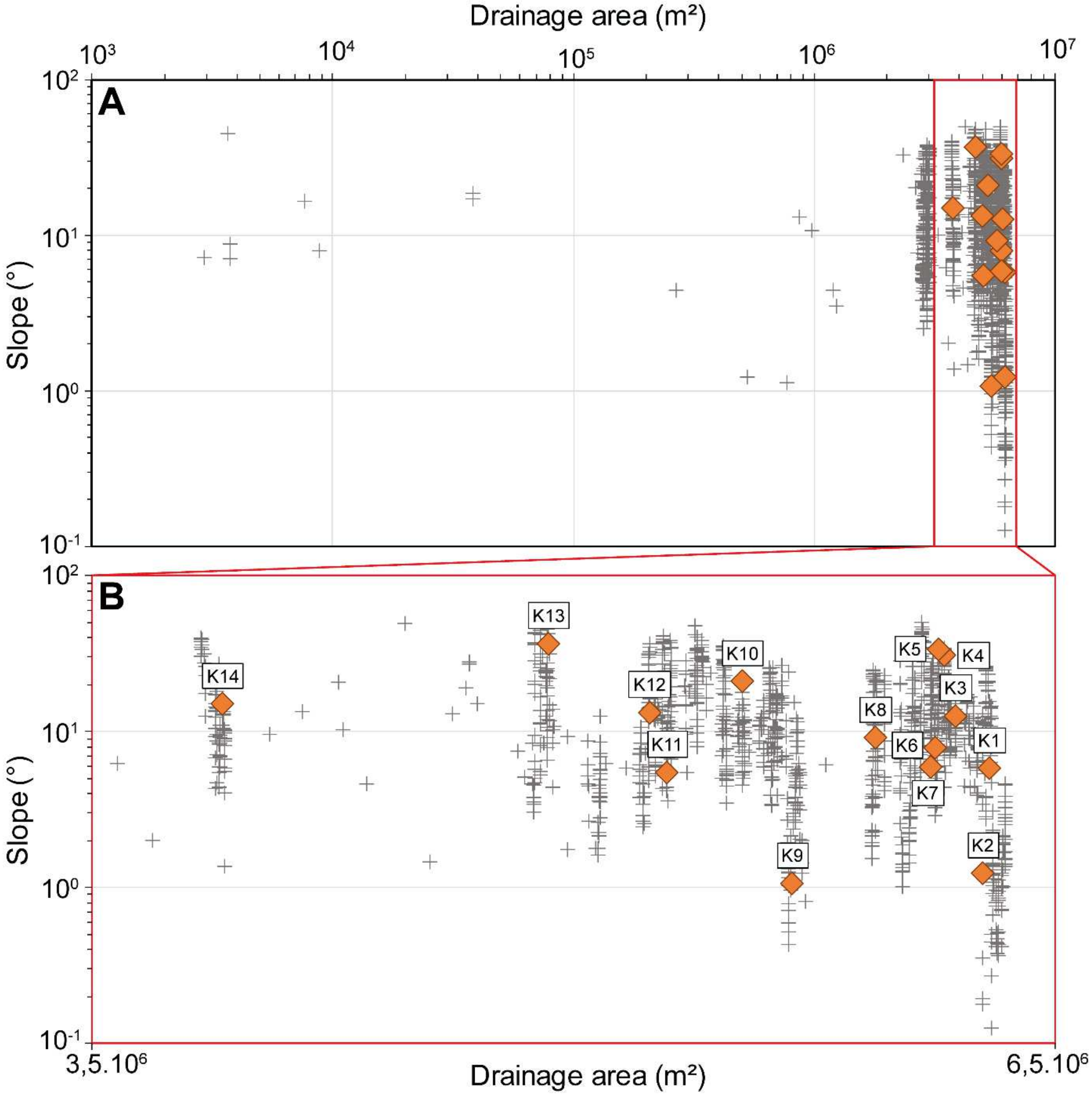

Fig. 9. Slope-area relationship ($\log_{10}$ scale) of river D1. **A)** Full set and **B)** Zoomed-in, with knickpoint values. Each grey cross corresponds to one pixel (4 m^2) along the stream profile of catchment D1.

The knickpoint activity (or inactivity) may be also highlighted by the values of the denudation rate deduced by the concentration of ^{36}Cl of the samples along stream D. During knickpoint activity, denudation rates should be higher downstream than upstream (e.g., Brocard et al., 2016). Instead, our results show that denudation rates do not vary between D4 and D2 despite the presence of knickpoints between these samples (Fig. 7B). Even more strikingly, the upstream sample, D5, presents a denudation rate higher than the downstream D4 sample (Fig. 7B), although this higher denudation rate could be enhanced by a local increase in stream flow and sediment supply due to the proximity of the sample to an upstream confluence and potential river capture event (Fig. 8B).

Only samples D2 and D1, upstream and downstream of K2 (which is associated with the post-MIS 5e regression) are in agreement with theoretical knickpoint dynamics (Fig. 7B). K2 would thus be the only knickpoint that is still active along the stream. It is another argument to suggest that the full propagation of eustatic knickpoints K13 to K3 was never reached, and knickpoints slowed down before that. A plausible explanation is that the small size of catchment D1 coupled with its partly karstic dynamics induces a low stream discharge and a low sediment supply, and thus an insufficient ability of the river to adjust to the base-level fall. This observation was already proposed by Castillo et al. (2013), who detected in Scotland a drainage area threshold of 4 km^2 for full knickpoint retreat. Another explanation for inhibition of knickpoint recession is the decreasing efficiency of the regressive erosion of the knickpoint produced by the decrease of the slope gradient downstream with the sea level rise during transgression. The transgression would erase the imbalance since the base level will almost return to its initial position (Fig. 1B). In addition, the knickpoints studied here are generated by a high-frequency external forcing (i.e. sea level variations; Fig. 7A), which does not allow them to adjust to the conditions before new ones appear.

5.1.3. Timescale of eustatic knickpoint retreat

The long-term horizontal propagation rate of the only knickpoint still active (i.e. K2), produced by the last major regression (i.e. MIS 5e), is ~1.71 $mm.a^{-1}$ (i.e. a retreat length of ~209 m in ~122 ka). The most likely hypothesis regarding the inactivity of knickpoints older than K2, is that a knickpoint slows down when a new one is formed by a new regression. To test such hypothesis, we quantified the correlation between the time interval between two interglacial highstands that enclose knickpoint formation and the knickpoint retreat length. However, no correlation between these two parameters was found ($R^2 = 0.04$; Fig. 10B). The propagation time of the knickpoints is shorter than the time intervals between two highstands.

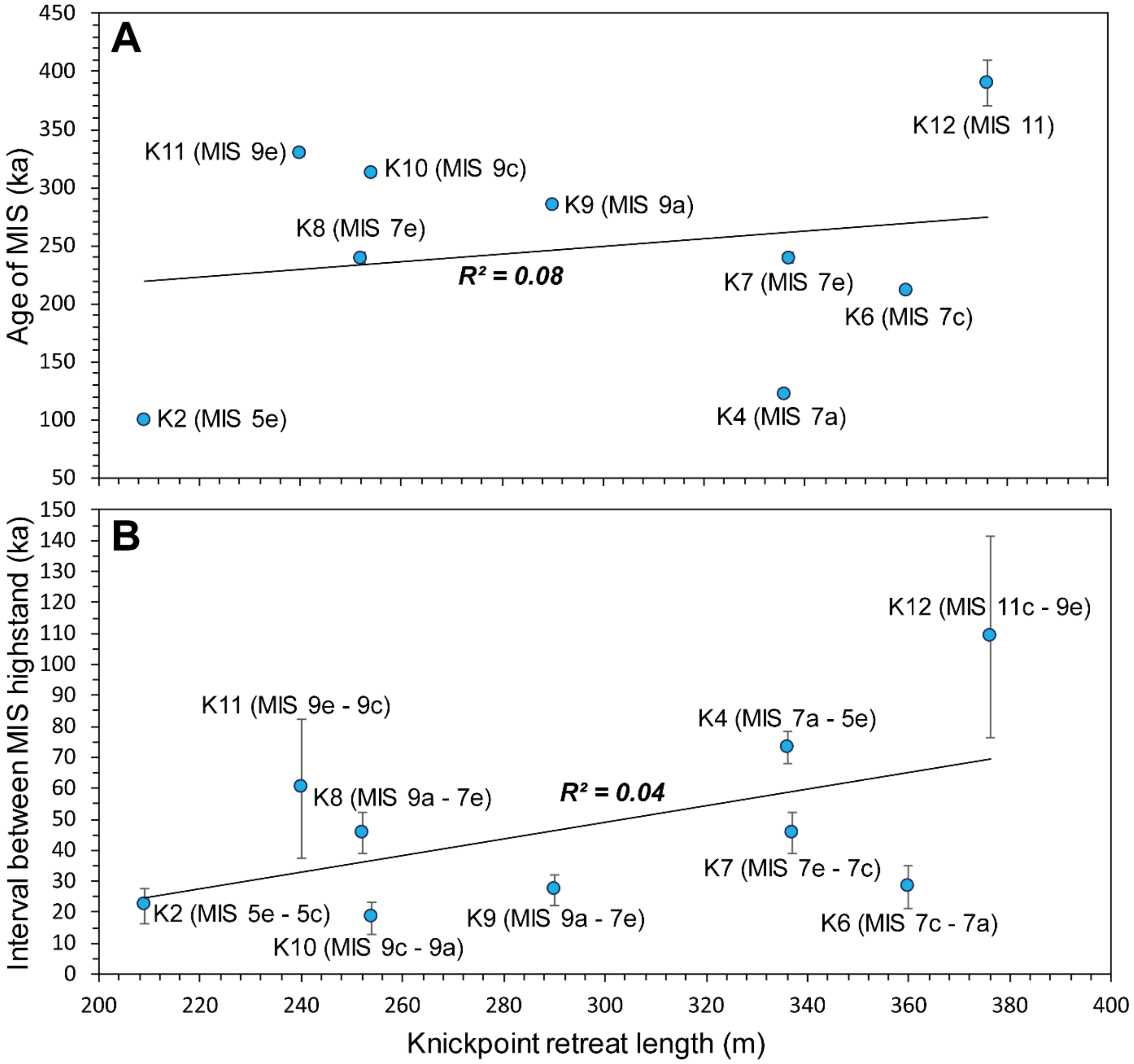

Fig. 10. Relationships between knickpoint retreat length calculated for the stream of catchment D1 with **A)** the corresponding highstand correlated to a MIS and **B)** the age interval between two successive highstands enclosing the knickpoint. The ages of MIS 11c, 9e, 9c, 9a, 7e, 7c, 7a, 5e, 5c and 5a are 390 ± 20, 330 ± 5, 312 ± 5, 285 ± 5, 239.5 ± 8.5, 211.5 ± 5.5, 195 ± 5, 122 ± 6, 100 ± 5 and 82 ± 3 ka, respectively (Cutler et al., 2003; Murray-Wallace and Woodroffe, 2014; Thompson and Goldstein, 2005).

Knickpoint migration rate depends on several parameters such as the drainage area, lithology and amplitude of base-level fall (e.g., Loget Van Den Driessche, 2009). The local stream gradient creating potential for abrasion, plucking and undercutting of bedrock and sediment supply could also impact this propagation rate (e.g., Whipple et al., 2013). Upstream of knickpoint K10, which is associated with the MIS 9c highstand, the stream gradient is high while it decreases downstream (Fig. 7C). However, the knickpoint retreat lengths of K11 and K13 are not greater than those of the lower downstream knickpoints. Thus, the local stream gradient does not seem to control the propagation rate. The knickpoint migration must vary according to other parameters, such as variations in regression/transgression rates or the geometry of the sequence that control the stream gradient during each regression. However, these forcings are difficult to constrain (e.g., Caputo, 2007). In addition, during Pleistocene regressions, the original offshore morphology of the foundations (i.e. the bedrock on which the reefs have been built over the last 1 Ma; Pirazzoli et al., 1993) has been obliterated by the construction of more recent reefs. In the end, our results only allow us to conclude that the timescale on which the knickpoint retreat is effective is short (i.e. a few thousand years).

5.2. Dynamics of coastal stream denudation

5.2.1. Vertical incision along the stream

In principle, at a constant incision rate, the older the incised CRT, the higher the finite vertical incision would be, which is at odds with our results (Fig. 7C). Besides, vertical incision does not increase significantly downstream of each knickpoint (Fig. 7C) which indicates that the incision induced by knickpoint retreat is negligible. Finite vertical incision values are comparable (~35 m) from the CRT associated with MIS 5e to the CRT associated with MIS 9c and increases upstream, with a maximum of ~74 m located at the distal part of the CRT associated with MIS 11c (Fig. 7B). Between MIS 11c CRT and MIS 9c CRT, the seaward slope of the sequence is higher than the seaward slope between the MIS 9c CRT and the MIS 5e CRT (Figs. 7B; 7C). We conclude that vertical incision rates are moderately influenced by eustatic knickpoint dynamics, but rather by the long wavelength slope gradient of the catchment.

5.2.2. Catchment scale denudation rates

For catchments located in a karstic environment, using the catchment area extracted from a DEM may be biased since a large part of this area may experience a much higher chemical weathering rate compared to the mechanical erosion rate (Authemayou et al., 2018). As a result, the denudation rates calculated in this study may be biased (section 3.2.). Nevertheless, we tried to compare the catchment- and canyon-scale CNC denudation rates with different uplift rates and morphometric parameters (i.e. drainage area, finite eroded volume, mean slope of canyon area, etc…) to appreciate the influence of these forcings on drainage dynamics (Table 1; Figs. 11A; 11B; 11C; 11D; 11E). However, in both cases (i.e. the relationships with CNC denudation rates of catchment or canyon area), there is no significant correlation of denudation rates with catchment and canyon areas, uplift rates, the finite eroded volume and the mean slope of canyons (Fig. 11). Moreover, we have previously shown that the denudation rate varies along the stream profile and that the catchment-scale denudation rate measured at the outlet mainly reflects the erosion of the last knickpoint associated with the eustatic drop of the last regression, especially if the outlet is close to the fossil sea cliff of the last emerged CRT. Thus, CNC denudation rates from the catchment outlet do not reflect the erosion process at the catchment scale, which prevents any possibility of seeing correlations with morphometric parameters.

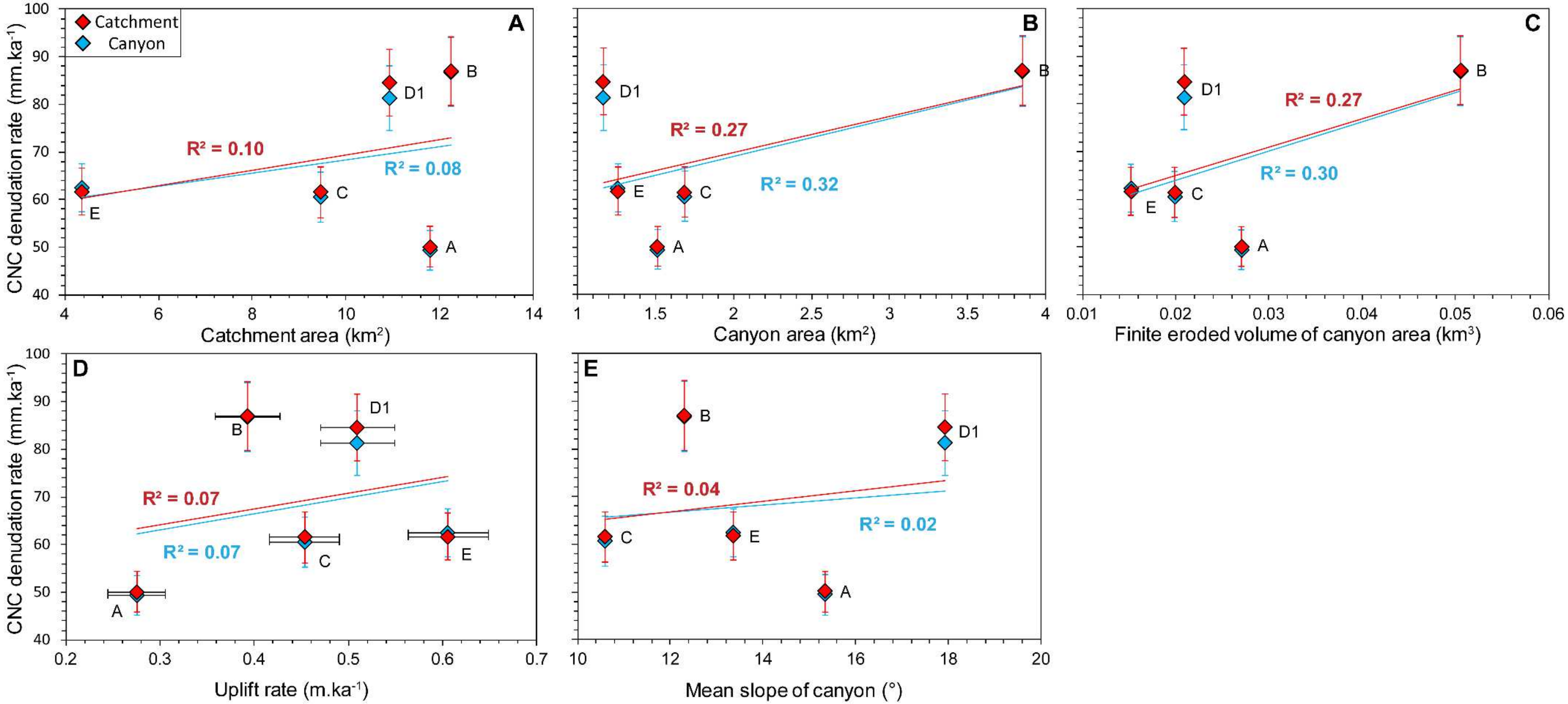

Fig. 11. Relationships between CNC denudation rate (calculated from the entire drainage area extracted automatically with the DEM (red diamond) and canyon area (blue diamond)), and **A)** Catchment area, **B)** Canyon area (incised zone), **C)** Finite eroded volume, **D)** Uplift rate, and **E)** Mean slope of canyon area.

5.2.3. Eroded volume at the catchment scale

Because the CNC denudation rate at the outlet is not representative of the catchment denudation, we compare the finite eroded volume at the catchment-scale obtained from catchments with different uplift rates and morphometric parameters (i.e. mean slope, drainage area, etc.) to assess their influence on the long-term drainage dynamics (Figs. 12A; 12B; 12C; 12D; 12E).

Firstly, there is no noticeable relationship between the finite eroded volumes, the CNC denudation rates (R^2=0.04) and the mean slope of the canyon areas (R^2=0.00; Figs. 12C; 12E). Nevertheless, we were able to observe a significant correlation between the finite eroded volumes and the area of catchments (R^2=0.79; Fig. 12A). Such correlation slightly decreases with the canyon area (R^2=0.49), but with a linear constraint on a single catchment (i.e. catchment B; Fig. 12B), excluding definitive conclusions regarding such correlations.

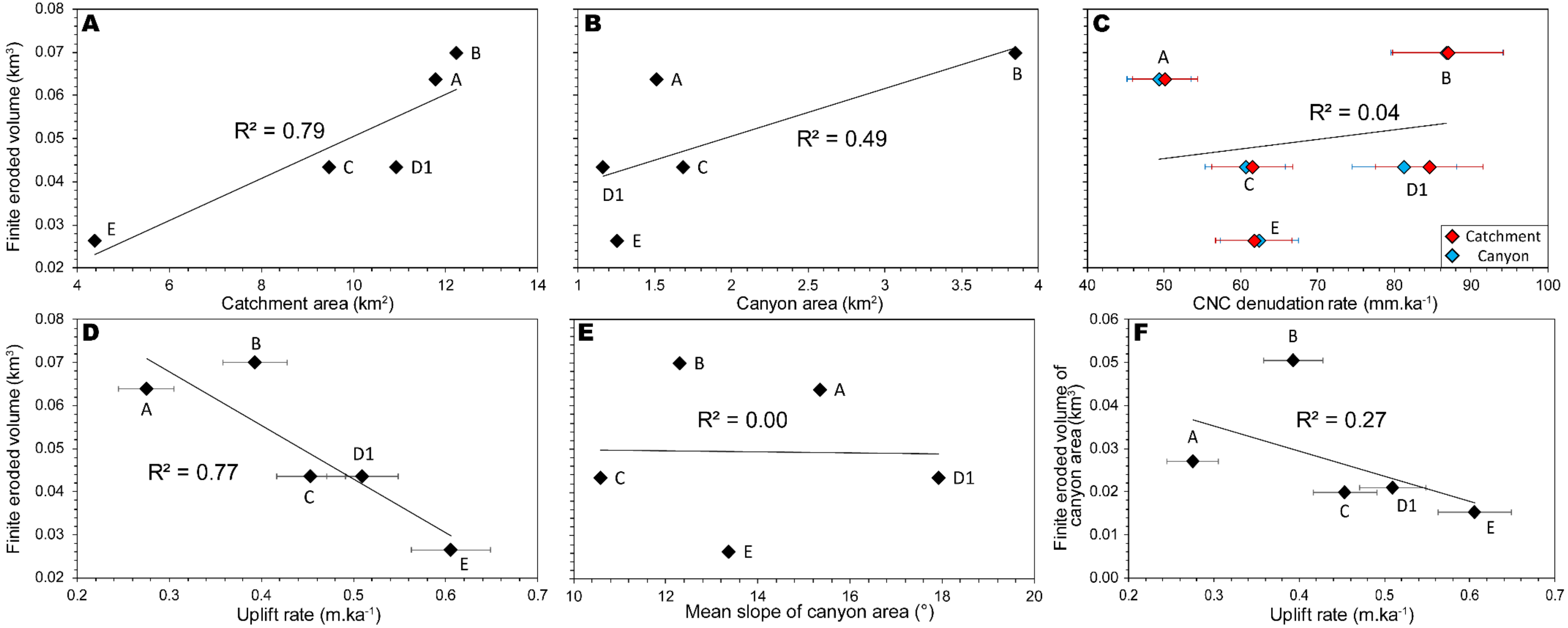

Fig. 12. Relationships between finite eroded volume and **A)** Catchment area, **B)** Canyon area (incised zone), **C)** CNC denudation rate, **D)** Uplift rate, and **E)** Mean slope of canyon area. **F)** Relationship between finite eroded volume of canyon area and uplift rate.

The finite eroded volumes and uplift rates also show a possible strong linear correlation (R^2=0.77; Fig. 12D). However, this relationship shows an inverse trend to what the stream power law predicts about the relationship between erosion and uplift rate in a steady state (e.g., Whipple, 2004; Wobus et al., 2006). The catchments affected by the highest uplift rates (D1 and E) show the lowest finite eroded volumes, while the catchments affected by the lowest uplift rates (A and B) have the highest finite eroded volumes (Fig. 12D). In addition, the catchments affected by low uplift rates are those with the largest total drained areas (Figs. 12A; 12B). These relationships would suggest that the lower the uplift rate, the more the catchment extends its drained area onto the CRTs surfaces near the canyon. This leads to an increase in sediment inputs from chemical weathering of the CRTs surfaces that contribute to the catchment supply, and thus an increase in the finite eroded volume (Figs. 12D; 12F). Such an observation is consistent with the results of Nexer et al. (2015) indicating that the more a catchment is located in an area of high uplift rate, the more elongated and the less widened it is (catchments D1 and E in figure 4). Its surface area thus remains small because it will tend to incise mainly along the main drainage of the catchment rather than expand laterally.

6. Conclusion

In Sumba Island, the specific morphology of the emerged coral reef terraces sequence, shaped by the combined effects of constant uplift rate and Quaternary sea-level fluctuations, yields a drainage network characterized by the formation of several knickpoints along coastal stream profiles. We correlated the formation of the majority of these knickpoints to major Quaternary Sea level highstands. Each knickpoint was formed at the distal edge of the reef recently emerged at the beginning of the regression. We highlight that the eustatic knickpoint retreat length does not depend on the age of knickpoint formation and are quite homogenous in the sequence drainage. These eustatic knickpoints migrate upstream until they almost stall before the next sea level transgression. The inability of the river to fully absorb the base-level fall would probably be related to its low stream discharge of small drainage areas, low sediment supply in karstic carbonated conditions of the coral reef terraces sequence, and the high frequency of the eustatic oscillations.

Catchment-scale denudation rates investigated from ^{36}Cl concentration on five catchments draining exclusively the sequence yielded an average value of 69 ± 16 mm.ka^{-1} (integrated over a few thousand years). No significant correlation was noticed between the catchments morphometric parameters, uplift and denudation rates because the denudation rate at the outlet influenced by the younger knickpoint activity is not representative of the catchment denudation rate. Also, the relationships between the finite eroded volumes of the catchments and the morphometric parameters highlight that slower uplift for a catchment may correspond to a greater finite eroded volume. This result is explained by the tendency of catchments to widen with low uplift rate and to lengthen while incising the sequence deeply with higher uplift rate.

Acknowledgements

This work was supported by public funds from the "Investissements d'Avenir" program managed by the French National Research Agency (ANR-10-EQPX-20 and ANR-10-LABX-19-01, Labex Mer, CLIMORESO, C. Authemayou), the INSU

Tellus Syter program (SECOMAS, C. Authemayou), and the CNES TOSCA program (CETTROPICO, C. Authemayou). We thank the German Aerospace Center to provide us the TanDEM-X data for our study area. We thank the State Ministry of Research and Technology of Indonesia “RISTEK” that allowed us to conduct the field trip to Sumba (research permit 680/FRP/E5/Dit.KI/IV/2017). We also thank the National Geographic Explorer grant (no CP 087R 17) to support the Indonesian researchers (Sri Yudawati Cahyarini). We thank David Fernández Blanco for the stacked swath profiles. We also thank the editor and reviewers for their recommendations and suggestions.

References cited

Abdullah, C. I., Rampnoux, J. P., Bellon, H., Maury, R. C., & Soeria-Atmadja, R. (2000). The evolution of Sumba Island (Indonesia) revisited in the light of new data on the geochronology and geochemistry of the magmatic rocks. Journal of Asian Earth Sciences, 18(5), 533-546.

Armijo, R., Lacassin, R., Coudurier-Curveur, A., & Carrizo, D. (2015). Coupled tectonic evolution of Andean orogeny and global climate. Earth-Science Reviews, 143, 1–35.

Authemayou, C., Brocard, G., Delcaillau, B., Molliex, S., Pedoja, K., Husson, L., et al. (2018). Unraveling the roles of asymmetric uplift, normal faulting and groundwater flow to drainage rearrangement in an emerging karstic landscape. Earth Surface Processes and Landforms, 43(9), 1885-1898.

Bard, E., Jouannic, C., Hamelin, B., Pirazzoli, P., Arnold, M., Faure, G., et al. (1996). Pleistocene sea levels and tectonic uplift based on dating of corals from Sumba Island, Indonesia. Geophysical Research Letters, 23(12), 1473-1476.

Berlin, M. M., & Anderson, R. S. (2007). Modeling of knickpoint retreat on the Roan Plateau, western Colorado. Journal of Geophysical Research: Earth Surface, 112(F3).

Bierman, P. R. (1994). Using in situ produced cosmogenic isotopes to estimate rates of landscape evolution: A review from the geomorphic perspective. Journal of Geophysical Research: Solid Earth, 99(B7), 13885-13896.

Bierman, P., & Steig, E. J. (1996). Estimating rates of denudation using cosmogenic isotope abundances in sediment. Earth Surface Processes and Landforms, 21(2), 125-139.

Boulton, S. J., & Stokes, M. (2018). Which DEM is best for analyzing fluvial landscape development in mountainous terrains?. Geomorphology, 310, 168-187.

Bowen, D.Q., (2010). Sea level ~ 400 000 years ago (MIS 11) : analogue for present and future sea-level ? Clim. Past 6, 19-29.

Braucher, R., Merchel, S., Borgomano, J., & Bourlès, D. L. (2011). Production of cosmogenic radionuclides at great depth: a multi element approach. Earth and Planetary Science Letters, 309(1-2), 1-9.

Brocard, G. Y., Willenbring, J. K., Scatena, F. N., & Johnson, A. H. (2016). Effects of a tectonically-triggered wave of incision on riverine exports and soil mineralogy in the Luquillo Mountains of Puerto Rico. Applied Geochemistry, 63, 586-598.

Brown, E. T., Stallard, R. F., Larsen, M. C., Raisbeck, G. M., & Yiou, F. o. (1995). Denudation rates determined from the accumulation of in situ-produced 10Be in the Luquillo Experimental Forest, Puerto Rico. Earth and Planetary Science Letters, 129(1-4), 193-202.

Cantelli, A., & Muto, T. (2014). Multiple knickpoints in an alluvial river generated by a single instantaneous drop in base level: experimental investigation. Earth Surface Dynamics, 2(1), 271-278.

Caputo, R. (2007). Sea-level curves: perplexities of an end-user in morphotectonic applications. Global and Planetary Change, 57(3-4), 417-423.

Castillo, M., Bishop, P., & Jansen, J. D. (2013). Knickpoint retreat and transient bedrock channel morphology triggered by base-level fall in small bedrock river catchments: the case of the Isle of Jura, Scotland. Geomorphology, 180, 1-9.

Castillo, M., Muñoz-Salinas, E., Ferrari, L., (2014). Response of a landscape to tectonics using channel steepness indices (ksn) and OSL: a case of study from the Jalisco Block, Western Mexico. Geomorphology 221, 204–214.

Champagnac, J. D., Molnar, P., Sue, C., & Herman, F. (2012). Tectonics, climate, and mountain topography. Journal of Geophysical Research: Solid Earth, 117(B2).

Chappell, J. (1974). Geology of coral terraces, Huon Peninsula, New Guinea: a study of Quaternary tectonic movements and sea-level changes. Geological Society of America Bulletin, 85(4), 553-570.

Chauveau, D., Authemayou, C., Pedoja, K., Molliex, S., Husson, L., Scholz, D., Godar, V., Pastier, A.M., de Gelder, G., Cahayarini, S.Y., Elliot, M., Weber, M., Benedetti, L., Jaud, M., Boissier, A., Agusta, V.C., Aribowo, S., Budd, A.F., Natawidjaja, D.H. (2021). On the generation and degradation of emerged coral reef terraces sequences: first cosmogenic ^{36}Cl analysis at Cape Laundi, Sumba Island (Indonesia). Quaternary Science Review. 269, 107144, ISSN 0277-3791. https://doi.org/10.1016/j.quascirev.2021.107144

Codilean, A. T. (2006). Calculation of the cosmogenic nuclide production topographic shielding scaling factor for large areas using DEMs. Earth Surface Processes and Landforms, 31(6), 785-794.

Crosby, B. T., & Whipple, K. X. (2006). Knickpoint initiation and distribution within fluvial networks: 236 waterfalls in the Waipaoa River, North Island, New Zealand. Geomorphology, 82(1-2), 16-38.

Cutler, K. B., Edwards, R. L., Taylor, F. W., Cheng, H., Adkins, J., Gallup, C. D., et al. (2003). Rapid sea-level fall and deep-ocean temperature change since the last interglacial period. Earth and Planetary Science Letters, 206(3-4), 253-271.

Dunai, T. J. (2010). Cosmogenic Nuclides: Principles, concepts and applications in the Earth surface sciences: Cambridge University Press.

Duvall, A., Kirby, E., Burbank, D., (2004). Tectonic and lithologic controls on bed-rock channel profiles and processes in coastal California. J. Geophys. Res. 109 (F3002), 1–18.

Fabryka-Martin, J.T., (1988). Production of radionuclides in the earth and their hydrogeologic significance, with emphasis on chlorine-36 and iodine-129. Ph.D. Thesis, Department of Hydrology and Water Resources, University of Arizona, Tucson, 400 pp.

Farber, D. L., Mériaux, A.-S., & Finkel, R. C. (2008). Attenuation length for fast nucleon production of 10Be derived from near-surface production profiles. Earth and Planetary Science Letters, 274(3-4), 295-300.

Fernández-Blanco, D., de Gelder, G., Lacassin, R., & Armijo, R. (2019). Geometry of flexural uplift by continental rifting in Corinth, Greece. Tectonics.

Fleury, J.-M., Pubellier, M., & de Urreiztieta, M. (2009). Structural expression of forearc crust uplift due to subducting asperity. Lithos, 113(1-2), 318-330.

Flint, J.J., (1974). Stream gradient as a function of order, magnitude, and discharge. Water Resour. Res. 10, 969–973.

Fortuin, A. R., Van der Werff, W., & Wensink, H. (1997). Neogene basin history and paleomagnetism of a rifted and inverted forearc region, on-and offshore Sumba, Eastern Indonesia. Journal of Asian Earth Sciences, 15(1), 61-88.

Gardner, T. W. (1983). Experimental study of knickpoint and longitudinal profile evolution in cohesive, homogeneous material. Geological Society of America Bulletin, 94(5), 664-672.

Godard, V., Dosseto, A., Fleury, J., Bellier, O., Siame, L., & Team, A. (2019). Transient landscape dynamics across the Southeastern Australian Escarpment. Earth and Planetary Science Letters, 506, 397-406.

Granger, D. E., Kirchner, J. W., & Finkel, R. (1996). Spatially averaged long-term erosion rates measured from in situ-produced cosmogenic nuclides in alluvial sediment. The Journal of Geology, 104(3), 249-257.

Granger, D. E., & Riebe, C. S. (2014). Cosmogenic nuclides in weathering and erosion.

Haig, D. W. (2012). Palaeobathymetric gradients across Timor during 5.7-3.3 Ma (latest Miocene-Pliocene) and implications for collision uplift. Palaeogeography, Palaeoclimatology, Palaeoecology, 331, 50-59.

Hall, R., & Smyth, H. R. (2008). Cenozoic arc processes in Indonesia: Identification of the key infuences on the stratigraphic record in active volcanic arcs. Formation and applications of the sedimentary record in arc collision zones, 436, 27.

Hantoro, W. S., Jouannic, C., & Pirazzoli, P. A. (1989). Terrasses coralliennes quaternaires soulevées dans l'île de Sumba (Indonésie) (full text in French, English and Spanish). Photo interprétation (Paris), 28(1), 17-34.

Hantoro, W. S. (1992). Etude des térraces récifales quaternaires soulévées entre le détroit de la sonde et l’île de Timor, Indonésie; mouvements verticaux de la croûte terrestre et variations de niveau de la mer. Ph.D. Thesis, Université d’Aix-Marseille 11.

Harris, R. A. (1991). Temporal distribution of strain in the active Banda orogen: a reconciliation of rival hypotheses. Journal of Southeast Asian Earth Sciences, 6(3-4), 373-386.

Hayakawa, Y., & Matsukura, Y. (2003). Recession rates of waterfalls in Boso Peninsula, Japan, and a predictive equation. Earth Surface Processes and Landforms: The Journal of the British Geomorphological Research Group, 28(6), 675-684.

Heisinger, B., Lal, D., Jull, A. J. T., Kubik, P., Ivy-Ochs, S., Neumaier, S., et al. (2002). Production of selected cosmogenic radionuclides by muons: 1. Fast muons. Earth and Planetary Science Letters, 200(3-4), 345-355.

Hinschberger, F., Malod, J.-A., Réhault, J.-P., Villeneuve, M., Royer, J.-Y., & Burhanuddin, S. (2005). Late Cenozoic geodynamic evolution of eastern Indonesia. Tectonophysics, 404(1-2), 91-118.

Jones, E. S., Hayes, G. P., Bernardino, M., Dannemann, F. K., Furlong, K. P., Benz, H. M., & Villaseñor, A. (2014). Seismicity of the Earth 1900–2012 Java and vicinity: U.S. Geological Survey Open-File Report 2010–1083-N, 1 sheet, scale 1:5,000,000.

Jouannic, C., Hantoro, W. S., Hoang, C. T., Fournier, M., Lafont, R., & Ichtam, M. L. (1988). Quaternary raised reef terraces at Cape Laundi, Sumba, Indonesia: geomorphological analysis and first radiometric (Th/U and 14C) age determinations. Presented at the Processing of the 6th International Coral Reef Symposium, Townsville, Australia (1988), 441-447.

Kirby, E., & Whipple, K. X. (2012). Expression of active tectonics in erosional landscapes. Journal of Structural Geology, 44, 54-75.

Korup, O., Montgomery, D.R., Hewitt, K., (2010). Glacier and landslide feedbacks to topographic relief in the Himalayan syntaxes. Proceedings of the National Academy of Sciences 107, 5317-5322.

Loget, N., & Van Den Driessche, J. (2009). Wave train model for knickpoint migration. Geomorphology, 106(3-4), 376-382.

Lucazeau, F., & Hurtrez, J. E. (1997). Length-scale dependence of relief along the south eastern border of Massif Central (France). Geophysical Research Letters, 24(14), 1823-1826.

Merchel, S., Arnold, M., Aumaître, G., Benedetti, L., Bourlès, D. L., Braucher, R., et al. (2008). Towards more precise 10Be and 36Cl data from measurements at the 10^{-14} level: influence of sample preparation. Nuclear Instruments and Methods in Physics Research Section B: Beam Interactions with Materials and Atoms, 266(22), 4921-4926.

Molliex, S. p., Rabineau, M., Leroux, E., Bourlès, D. L., Authemayou, C., Aslanian, D., et al. (2016). Multi-approach quantification of denudation rates in the Gulf of Lion source-to-sink system (SE France). Earth and Planetary Science Letters, 444, 101-115.

Montgomery, D. R., & Brandon, M. T. (2002). Topographic controls on erosion rates in tectonically active mountain ranges. Earth and Planetary Science Letters, 201(3-4), 481-489.

Murray-Wallace, C. V., & Woodroffe, C. D. (2014). Quaternary sea-level changes: a global perspective: Cambridge University Press. 276, 314-316.

Nexer, M., Authemayou, C., Schildgen, T., Hantoro, W. S., Molliex, S., Delcaillau, B., et al. (2015). Evaluation of morphometric proxies for uplift on sequences of coral reef terraces: A case study from Sumba Island (Indonesia). Geomorphology, 241, 145-159.

Nugroho, H., Harris, R., Lestariya, A. W., & Maruf, B. (2009). Plate boundary re-organization in the active Banda Arc-continent collision: Insights from new GPS measurements. Tectonophysics, 479(1-2), 52-65.

Pedoja, K., Regard, V., Husson, L., Martinod, J., Guillaume, B., Fucks, E., et al. (2011). Uplift of Quaternary shorelines in eastern Patagonia: Darwin revisited. Geomorphology, 127(3-4), 121-142.

Pedoja, K., Husson, L., Johnson, M. E., Melnick, D., Witt, C., Pochat, S. p., et al. (2014). Coastal staircase sequences reflecting sea-level oscillations and tectonic uplift during the Quaternary and Neogene. Earth-Science Reviews, 132, 13-38.

Pedoja, K., Husson, L., Bézos, A., Pastier, A.-M., Imran, A. M., Arias-Ruiz, C., et al. (2018). On the long-lasting sequences of coral reef terraces from SE Sulawesi (Indonesia): Distribution, formation, and global significance. Quaternary Science Reviews, 188, 37-57.

Phillips, F. M., & Plummer, M. A. (1996). CHLOE; a program for interpreting in-situ cosmogenic nuclide data for surface exposure dating and erosion studies. Radiocarbon (Abstr. 7th Int. Conf. Accelerator Mass Spectrometry), vol. 38(1), 98-99.

Phillips, F. M., Stone, W. D., & Fabryka-Martin, J. T. (2001). An improved approach to calculating low-energy cosmic-ray neutron fluxes near the land/atmosphere interface. Chemical Geology, 175(3-4), 689-701.

Pirazzoli, P. A., Radtke, U., Hantoro, W. S., Jouannic, C., Hoang, C. T., Causse, C., et al. (1991). Quaternary raised coral-reef terraces on Sumba Island, Indonesia. Science, 252(5014), 1834-1836.

Pirazzoli, P. A., Radtke, U., Hantoro, W. S., Jouannic, C., Hoang, C. T., Causse, C., et al. (1993). A one million-year-long sequence of marine terraces on Sumba Island, Indonesia. Marine Geology, 109(3-4), 221-236.

Pirazzoli, P. A. (2005). A review of possible eustatic, isostatic and tectonic contributions in eight late-Holocene relative sea-level histories from the Mediterranean area. Quaternary Science Reviews, 24(18-19), 1989-2001.

Prasetia, R., As-syakur, A. R., & Osawa, T. (2013). Validation of TRMM Precipitation Radar satellite data over Indonesian region. Theoretical and applied climatology, 112(3-4), 575-587.

Reinhardt, L. J., Bishop, P., Hoey, T. B., Dempster, T. J., & Sanderson, D. C. W. (2007). Quantification of the transient response to base-level fall in a small mountain catchment: Sierra Nevada, southern Spain. Journal of Geophysical Research: Earth Surface, 112(F3).

Roep, T. B., & Fortuin, A. R. (1996). A submarine slide scar and channel filled with slide blocks and megarippled Globigerina sands of possible contourite origin from the Pliocene of Sumba, Indonesia. Sedimentary Geology, 103(1-2), 145-160.

Rutherford, E., Burke, K., Lytwyn, J., (2001). Tectonic history of Sumba Island, Indonesia, since the Late Cretaceous and its rapid escape into the forearc in the Miocene. J. Asian Earth Sci. 19 (4), 453–479.

Schimmelpfennig, I., Benedetti, L., Finkel, R., Pik, R. I., Blard, P.-H., Bourles, D., et al. (2009). Sources of in-situ 36Cl in basaltic rocks. Implications for calibration of production rates. Quaternary Geochronology, 4(6), 441-461.

Schimmelpfennig, I., Benedetti, L., Garreta, V., Pik, R., Blard, P.-H., Burnard, P., et al. (2011). Calibration of cosmogenic 36Cl production rates from Ca and K spallation in lava flows from Mt. Etna (38 N, Italy) and Payun Matru (36 S, Argentina). Geochimica et cosmochimica acta, 75(10), 2611-2632.

Schimmelpfennig, I., Schaefer, J. M., Putnam, A. E., Koffman, T., Benedetti, L., Ivy-Ochs, S., et al. (2014). 36Cl production rate from K-spallation in the European Alps (Chironico landslide, Switzerland). Journal of Quaternary Science, 29(5), 407-413.

Schlagenhauf, A., Gaudemer, Y., Benedetti, L., Manighetti, I., Palumbo, L., Schimmelpfennig, I., et al. (2010). Using in situ Chlorine-36 cosmonuclide to recover past earthquake histories on limestone normal fault scarps: a reappraisal of methodology and interpretations. Geophysical Journal International, 182(1), 36-72.

Schoenbohm, L. M., Whipple, K. X., Burchfiel, B. C., & Chen, L. (2004). Geomorphic constraints on surface uplift, exhumation, and plateau growth in the Red River region, Yunnan Province, China. Geological Society of America Bulletin, 116(7-8), 895-909.

Schumm, S. A. (1993). River response to baselevel change: implications for sequence stratigraphy. The Journal of Geology, 101(2), 279-294.

Small, E. E., & Anderson, R. S. (1998). Pleistocene relief production in Laramide mountain ranges, western United States. Geology, 26(2), 123-126.

Snyder, N.P., Whipple, K.X., Tucker, G.E., Merritts, D.J., (2000). Landscape response to tectonic forcing: digital elevation model analysis of streamprofiles in the Mendocino triple junction region, northern California. Geol. Soc. Am. Bull. 112 (8), 1250–1263.

Snyder, N. P., Whipple, K. X., Tucker, G. E., & Merritts, D. J. (2002). Interactions between onshore bedrock-channel incision and nearshore wave-base erosion forced by eustasy and tectonics. Basin Research, 14(2), 105-127.

Stone, J., Allan, G. L., Fifield, L. K., Evans, J. M., & Chivas, A. R. (1994). Limestone erosion measurements with cosmogenic chlorine-36 in calcite-preliminary results from Australia. Nuclear Instruments and Methods in Physics Research Section B: Beam Interactions with Materials and Atoms, 92(1-4), 311-316.

Stone, J. O., Allan, G. L., Fifield, L. K., & Cresswell, R. G. (1996). Cosmogenic chlorine-36 from calcium spallation. Geochimica et Cosmochimica Acta, 60(4), 679-692.

Thompson, W.G., Goldstein, S.L., (2005). Open-system coral ages reveal persistent suborbital sea-level cycles. Science 308 (5720), 401-404.

Vermeesch, P. (2007). CosmoCalc: An Excel add-in for cosmogenic nuclide calculations. Geochemistry, Geophysics, Geosystems, 8(8).

Von Blanckenburg, F. (2005). The control mechanisms of erosion and weathering at basin scale from cosmogenic nuclides in river sediment. Earth and Planetary Science Letters, 237(3-4), 462-479. https://doi.org/10.1016/j.epsl.2005.06.030

Waelbroeck, C., Labeyrie, L., Michel, E., Duplessy, J. C., McManus, J. F., Lambeck, K., et al. (2002). Sea-level and deep water temperature changes derived from benthic foraminifera isotopic records. Quaternary Science Reviews, 21(1-3), 295-305.

Whipple, K.X., (2004). Bedrock rivers and the geomorphology of active orogens. Annual Review of Earth and Planetary Sciences 32, 151-185.

Whipple, K. X., & Tucker, G. E. (1999). Dynamics of the stream-power river incision model: Implications for height limits of mountain ranges, landscape response timescales, and research needs. Journal of Geophysical Research: Solid Earth, 104(B8), 17661-17674.

Whipple, K. X., & Tucker, G. E. (2002). Implications of sediment-flux-dependent river incision models for landscape evolution. Journal of Geophysical Research: Solid Earth, 107(B2), ETG 3-1-ETG 3-20.

Whipple, K. X., Dibiase, R. A., & Crosby, B. T. (2013). Bedrock rivers. In Treatise on geomorphology (pp. 550-573): Elsevier Inc.

Whittaker, A. C., & Boulton, S. J. (2012). Tectonic and climatic controls on knickpoint retreat rates and landscape response times. Journal of Geophysical Research: Earth Surface, 117(F2).

Willenbring, J. K., Gasparini, N. M., Crosby, B. T., & Brocard, G. (2013). What does a mean mean? The temporal evolution of detrital cosmogenic denudation rates in a transient landscape. Geology, 41(12), 1215-1218.

Wobus, C., Whipple, K. X., Kirby, E., Snyder, N., Johnson, J., Spyropolou, K., et al. (2006). Tectonics from topography: Procedures, promise, and pitfalls. S.D. Willett, N. Hovius, M.T. Brandon, D.M. Fisher (Eds.), Tectonics, Climate, and Landscape Evolution, Geological Society of America Special Paper, vol. 398 (2006), 55-74.

Ye, F.-Y., Barriot, J.-P., & Carretier, S. (2013). Initiation and recession of the fluvial knickpoints of the Island of Tahiti (French Polynesia). Geomorphology, 186, 162-173.